UHASSELT
KNOWLEDGE IN ACTION

Maastricht University

Faculty of Medicine and Life Sciences
School for Life Sciences
Master of Biomedical Sciences

Masterthesis

Development of Multifunctional Resins for 3D Microprinting Applications

Joren Van Herck

Thesis presented in fulfillment of the requirements for the degree of Master of Biomedical Sciences, specialization Bioelectronics and Nanotechnology

SUPERVISOR :
Prof. dr. Tanja JUNKERS

CO-SUPERVISOR :
Prof. Dr. Pamela HABIBOVIC
Dr. David BARATA

MENTOR :
De heer Gijs RAMAKERS

2017
2018

Transnational University Limburg is a unique collaboration of two universities in two countries: the University of Hasselt and Maastricht University.

UHASSELT
KNOWLEDGE IN ACTION

www.uhasselt.be
Universiteit Hasselt
Campus Hasselt:
Martelarenlaan 42 | 3500 Hasselt
Campus Diepenbeek:
Agoralaan Gebouw D | 3590 Diepenbeek

UHASSELT
KNOWLEDGE IN ACTION

Maastricht University

Faculty of Medicine and Life Sciences
School for Life Sciences
Master of Biomedical Sciences

Masterthesis

Development of Multifunctional Resins for 3D Microprinting Applications

Joren Van Herck

Thesis presented in fulfillment of the requirements for the degree of Master of Biomedical Sciences, specialization Bioelectronics and Nanotechnology

SUPERVISOR :
Prof. dr. Tanja JUNKERS

CO-SUPERVISOR :
Prof. Dr. Pamela HABIBOVIC
Dr. David BARATA

MENTOR :
De heer Gijs RAMAKERS

Foreword & acknowledgement

In 2013, I started my study career in Diepenbeek, Hasselt as a biomedical student. Back then, I would never had thought that I would do my senior internship in a polymer lab. However, throughout the years, my inters in chemistry was growing as I did also my bachelor stage in the PRD group. Now, 5 years later, I look back at memorable moments, both scientific and non-scientific. Before moving on the scientific data, I would like to thank some people.

First of all, I would like to thank my promotor, Prof. Dr. Tanja Junkers. She gave me the opportunity to start this project in collaboration with Maastricht University. Despite the fact that we were litterly on the other side of the world, the communication went very well, either via skype meetings or via mail traffic. The monthly discussion gave me each time new insights into the project. Thank you!

Secondly, I thank my daily supervisor in Hasselt, Gijs. He gave me tips and tricks for optimal lab practice. Also the scientific discussion were always very useful. Subsequently, I thank my supervisor in Maastricht, David. He introduced me to a lot of new people in the MERLN institute. Scientifically, he came up with some very nice ideas and insight for the project, especially on the cell part.

I cannot forget all the people who helped me with data analysis and small lab problems; my fellow student Emma for the discussion in our small office, Lowie for the ESI-MS measurements and their interpretation, Arne for the help with my first column, all the people in the G83 lab for small question,…

I would also like to thank some people who had not directly contributed to the scientific part but really helped me a lot throughout this internship. Thank you Chris for the car I could borrow the last half year. This made the trips to Maastricht a lot easier. Thank you S.C. HOCKEY for unforgettable moments the last 4 years. Thank you to all my fellow students for the pleasant times after working hours.

Lastly, I will thank the most important persons, my family and my girlfriend. They supported me every minute of my time as student.

List of abbreviations

2D	Two Dimensional
2PA	Two Photon Absorption
2PP	Two-Photon Polymerization
3D	Three Dimensional
ATRP	Atom Transfer Radical Polymerization
CAD	Computer Aided Design
CDP	4-cyano4-[(dodecylsulfanylthiocarbonyl)sulfanyl]pentanoic acid
CRP	Controlled Radical Polymerization
DCC	N,N'-dicyclohexylcarbodi-imide
DMA	N,N-dimethylacrylamide
DMPA	2,2-dimethoxy-2-phenylacetophenone
DMSO	Dimethylsulfoxide
DP	Degree of Polymerization
ECM	Extracellular Matrix
GM	Göppert-Meyer
IR	Infrared
MMA	Methyl Methacrylate
NMP	Nitrogen Mediated Polymerization
pMMA	poly(Methyl Methacrylate)
PRD	Polymer Reaction Design
RAFT	Reversible Addition Fragmentation chain Transfer
TEGDA	Tetra(ethylene glycol) diacrylate
TRIM	Trimethylolpropane Trimethacrylate
UV	Ultraviolet

Table of Contents

Abstract

In the field of tissue regeneration and regenerative medicine, polymers are widely used for the manufacturing of scaffolds. Instructive structures, based on crosslinked polymers are expected to provide a proper environment for proliferation, migration and differentiation of the embedded cells/tissue. In order to mimic the natural extracellular matrix (ECM), the scale of the scaffolding needs to be in the micron range. Unlike conventional printing techniques, two photon polymerization (2PP) is capable of creating micro- (and even nano-) sized three-dimensional features with high resolution. In general, commercially available resins for 2PP lack the ability to be chemically post-modified. Also, mechanical properties are difficult to tune. Especially, post-modification reactions might be very useful in the coupling of growth factors onto the scaffolds, which can lead to an even higher control over cell behavior.

In this master thesis, the synthesis of photocurable resins for two photon polymerization was investigated. Besides crosslinker molecules and a photoinitiator, polymers were added to the mixture. These polymers were synthesized *via* an iniferter mechanism in a flow-setup. This variant of RAFT polymerization provide high end-group fidelity of the polymers, whereas the specific setup ensures reproducibility and facilitates upscaling of the synthesis. The preservation of the RAFT end-groups is especially of great interest since it allows post-modification of the polymers. Resins, which include such polymers, were crosslinked in the 2PP process yielding microstructures with the end-groups onto the surface. Preliminary studies were performed to study the viability and attachment of osteoblastic cells to the printed structures. In the future, *via* specific chemical reactions, growth factors or peptides will be attached onto the scaffolds. Such multifunctional scaffolds aim to provide a more realistic model of the ECM and improve tissue regeneration processes.

Samenvatting

Polymeren worden veelvuldig gebruikt in het maken van scaffolds voor weefsel regeneratie toepassingen. Van deze polymeer structuren wordt verwacht dat ze de ingebedde cellen/weefsels voorzien van een geschikte omgeving voor differentiatie, proliferatie en migratie. Omdat het nabootsen van de extracellulaire matrix (ECM) belangrijk is, moet de grootteorde van de scaffolds in de micrometer range liggen. Twee photon polymerisatie (2PP) kan zulke micro- (en zelfs nano-) 3D structuren maken met een hoge resolutie, iets waar andere print technieken in falen. Maar over het algemeen missen de commerciële 2PP resins de mogelijkheid om de structuren te modificeren. Ook de variatie in mechanische eigenschappen is een tekortkoming van deze resins. Vooral de post-modificatie reacties kunnen van zeer groot nut zijn omdat we dan groei factoren kunnen koppelen op de scaffolds. Dit zou op zijn beurt kunnen leiden tot een nog hogere controle in cel gedrag in tissue engineering toepassingen.

In deze masterscriptie werd de synthese van een lichtgevoelige resin voor 2PP onderzocht. Naast crosslinkers en een photoinitiator werden nu ook polymeren toegevoegd aan het mengsel. Deze polymeren werden gemaakt via een iniferter mechanisme in een flow opstelling. De RAFT polymerisatie zorgt voor een hoog behoud van eind-groepen en de flow opstelling verhoogt de reproduceerbaarheid en vergemakkelijkt upscaling van de synthese. Vooral het behoud van de eind-groepen is hier van belang omdat we *via* deze groepen post-modificaties kunnen doen. Dus resins met deze polymeren werden gecrosslinked in het 2PP proces. Deze microstructuren hebben nu de eind-groepen van de polymeren op hun oppervlakte. Korte inleidende studies over de aanhechting en leefbaarheid van osteoblasten werden uitgevoerd. Door de eind-groepen op de oppervlakten is nu mogelijk om via allerhande reacties groeifactoren, peptiden of andere chemicaliën te koppelen op de structuren. Deze multifunctionele scaffolds hebben het doel om een meer realistisch model van het ECM te vormen en op deze manier het weefsel regeneratie proces te verbeteren.

Chapter I – Introduction

1.1 Biomedical need for new materials

Injury or diseases can lead to degeneration of organ and tissue. Some of our organs are known for their high rate of regeneration, like the liver. Other important organs have a relatively limited ability of self-healing, like the heart.[1] In these cases, the loss of the tissue function can be solved by replacing the whole organ by a donor organ. Due to the modern medicine, our population is ageing, which leads to increasing numbers of organ failures and thereby, longer waiting lists for organ donors. New techniques must be introduced to answer this increasing organ donor demand.[2]

Throughout the years, combined knowledge of cell biology, cell transplantation, chemistry and biomaterials has led to new insights and techniques in the field of tissue regeneration. This branch of modern medicine deals with the creation of functional tissues. According to literature, the three important components for tissue engineering, the so-called 'tissue engineering triad', are (stem)cells, growth factors and a biomaterial that serves as a scaffold.[3] A lot of ongoing research deals with the biocompatibility of different biomaterials, while other research focusses on the structural influences of the scaffold onto cells.[4] The main idea of these scaffolds is to embed the cells in a way that mimics the extracellular matrix (ECM). Therefore, a couple of requirements must be met for developing a good scaffold. Firstly, for the majority of tissues, the scaffolds needs to be a 3D matrix, to create a microenvironment that more closely mimics the physiological situation than the current cell culture models using 2D-monolayer cell growth in petri/multiwell.[5] Secondly, important for efficient release of biological growth factors and proper nutrient exchange, porosity and pore size of the 3D matrix is of great interest. Ma *et al.* showed that low porosity of the scaffold increases the cell proliferation rate whereas high porosity leads to a higher degree of cell differentiation.[6] For this reason, control of porosity parameters cannot be underestimated. On top of these geometrical concerns, the material needs to be biocompatible, i.e. proper adhesion and normal functioning of the embedded cells.

1.2 Microscale scaffolds by 2PP

Two main categories of 3D scaffold manufacturing techniques can be distinguished: porogen-based fabrication techniques and computer-aided design (CAD) techniques. Porogen-based fabrication techniques like solvent-casting[7], gas foaming[8], phase separation[9], or melt molding[10] are all based on a common principle. A polymer with incorporated porogen particles is synthesized into the right three-dimensional geometry. Subsequently, removal of the porogen leads to the creation of a porous structure. However, the control of pore size, pore geometry and pore interconnectivity is not accurate. As mentioned before, these properties are crucial for optimal cell ingrowth. In addition, the use of toxic solvents and a limited variation of mechanical properties forces science to seek for better alternatives.[11] In the late 80s of the previous century, the first 3D structures were made using CAD techniques, namely stereolithography.[12] This technique uses an ultraviolet (UV) laser to photopolymerize a liquid resin. Upon irradiation, the liquid polymeric solution is solidified in a

layer-by-layer approach. After removal of the excess non-reacted resin, 3D structures are obtained. Despite improvements in speed and reproducibility of the manufacturing procedure, the smallest pore size reached, which is between 50-100 µm, is still not optimal for proper scaffolding of tissues.[13] Further increasing the resolution and decreasing the smallest feature size can lead to better control over cell behavior in tissue regeneration applications. A relatively new principle, called two-photon polymerization (2PP), was introduced in the field of scaffold engineering in the beginning of the 21st century. With this technique, structures at the (sub)micron scale can be created.

Two-photon polymerization is based on two-photon absorption (2PA). Whereas normal light absorption needs a single photon to excite a molecule from the ground state to an excited state, 2PA uses two photons to do this. The first photon excites the molecule to a virtual intermediate energy level, the absorption of the second photon leads to excitation to a real higher energy state. The sum of the energy of these two photons is the same as the energy of one photon that induces the same process.[14] Translating this to a practical example: the energy of one UV photon is the same as the energy of two infrared (IR) photons:

$$E = h\nu_{UV} = \frac{1}{2}h\nu_{IR} + \frac{1}{2}h\nu_{IR} \qquad \text{(Equation 1)}$$

where E is the energy, h is the Planck constant and ν is the frequency.

After excitation to a higher energy state, the molecule can undergo rapid non-radiative relaxation, *i.e.* inter-system crossing, resulting in radical generation and polymerization initiation. For 2PP initiating molecules, the fluorescence quantum yield should be as low as possible as relaxation *via* fluorescence is in competition with radical formation (Figure 1).[15]

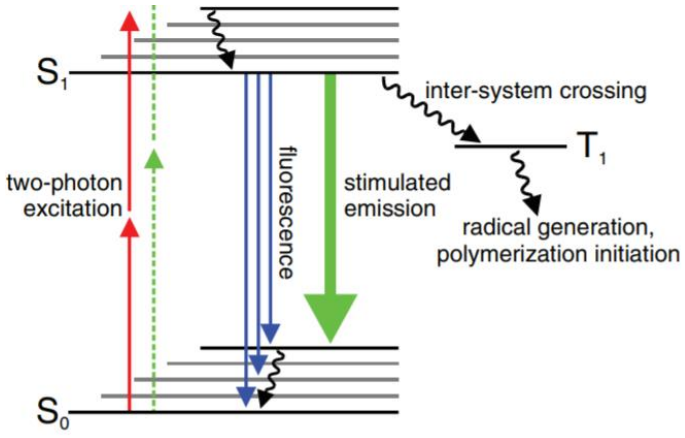

Figure 1 Jablonksi diagram shows the photochemical procceses in two-photon polymerization (2PP).[15]

Since the lifetime of the virtual intermediate energy level is very short (10^{-4} - 10^{-9} s), one requirement for 2PA is an almost simultaneously absorption of the two photons. This is achieved by using an ultrashort pulsed laser rather than a high powered continuous wave laser. Since the concentration of photons in one point in time is now much higher, the probability of a 2PA event also increases. Moreover, this 2PA response is proportional to the second power of the photon flux density, i.e. intensity. This results in a quadratic dependency which leads to highly spatial control of the

photopolymerization. Together with the fact that IR photons show high penetrability inside the polymeric resins, this phenomenon results in real 3D printing inside the liquid resin. This is in contrast with the layer-by-layer approach of other CAD techniques like stereolithography.

In a typical 2PP setup, i.e. for instance Nanoscribe (GmbH, Photonic Professional), a femtosecond laser source is focused into a photocurable resin. With a motorized coarse stage and a piezo stage for fine positioning, the resin can be moved in all three spatial dimension in order to photopolymerize true 3D features. The resin is mainly crosslinked in the focal point of the laser which is ellipsoid in shape, i.e. voxel. These voxels can be seen as the building blocks of the structures and their dimensions are therefore the limitations of the resolution. These resolution confinements are in contrast with conventional one-photon polymerization were the wavelength of the light and the numerical aperture of the system is responsible for the maximum obtained resolution, i.e. diffraction limit. Since the formation of voxels have a threshold response (simultaneously absorption of two photons) to light excitation, the diffraction limit does not put an actual restraint on voxel size in 2PP. Therefore, structures can be made beyond this diffraction limit.[16]

1.3 New resin formulations

Commercial 2PP resins are available in different compositions. Recently, researchers have also tried to develop customized resins tailored to a specific application.[17] For both the commercial and the in house-made resins, a crosslinking monomer and a 2PA photoinitiator are required to allow 2PP. The crosslinking monomers are the building blocks of the structures. They provide dense polymeric networks and determine the structural properties of the final structures. In general, acrylic crosslinkers are used for this purpose since they are known for their rapid propagation.[18] For such monomers to react, a source of radicals is needed. The pool of radicals is provided by the 2PA photoinitiator. Although the concentration is mostly very low, these 2PA photoinitiator molecules play a key role in the 2PP process. The efficiency of 2PA is therefore highly important and needs to be as high as possible. Quantitively, this efficiency in non-linear photon absorption is given by the 2PA cross section σ and is measured in Göppert-Meyer (GM) units [10^{-50} cm^4 s $photon^{-1}$]. In the early stages of the development of 2PP, 2PA active chromophores were explored as photoinitiator. Although ideal for bioimaging applications, these molecules are not capable of inducing effective photopolymerization. This is because, ideally, 2PP photoinitiators have low fluorescence quantum yields, since fluorescence is a relaxation process in competition with inter-system crossing, and thus radical formation. Throughout the years, various self-made 2PP photoinitiators were developed with high σ values but low fluorescence quantum yields.[19] According to the literature, high σ values are related to charge transfer characteristics of the molecule. Therefore, mostly centrosymmetric molecules with electron-donating (D) and electron-withdrawing (A) moieties separated by a conjugated π-electron system are synthesized and used for 2PP applications. Highly efficient 2PP photoinitiators have σ values of 100 GM or higher.[20]

Although the manufacturing of large structures with a submicron dimension is not yet realistic due to practical considerations of the commercial 2PP device, *i.e.* such as Nanoscribe (GmbH, Photonic Professional), the importance of micropatterning in biomedical applications has already been explored. Already in the early years of tissue engineering, researchers investigates the influences of

topological features on cell behavior.[21] For example, Barata *et al.* showed the importance of topological feature dimensions on the behavior of adherent cells. They showed that pillars of 2,5 micrometers in height exhibited cell spreading over the structures, whereas a constant height of 3 micrometers resulted in cell confinement between the pillars, rarely covering them.[22] Besides topological influences on cell behavior, cell growth control can also be achieved by the incorporation of growth factors into the system. For example, Hahn *et al.* directed cell growth in a certain way by coupling growth factors into a hydrogel matrix.[23] By combining micropatterning and growth factor incorporation in tissue regeneration applications, it is hypothesized that a higher level of cell fate control can be achieved.

As was mentioned earlier, 2PP is capable of fabricating features with a very high resolution, up to a few micrometers, and even nanometers. However, most commercial polymeric resins used for 2PP do not have the ability to post-modify these final microstructures. Such alterations onto a micropattern can be of great interest, since growth factors or peptides can be chemically attached to influence cell migration, proliferation and differentiation. Therefore, a 2PP resin composition which allows post-modification of the final structures can be of great interest in tissue engineering applications. In order to realize this, polymers are added as an additional ingredient to a mixture of acrylic crosslinker and 2PA photoinitiator. By synthesizing these polymers *via* a controlled radical polymerization (CRP), high end-group fidelity is ensured which make post-modification *via* these end-groups possible. By using CRP as the polymerization technique, control over the molecular weight distribution and chain length of the polymer is obtained. Hereby, it is possible to control the solubility of the polymer in the mixture and finetune the viscosity of the final resin. Also, by using a continuous flow setup, upscaling of the procedure should be more straightforward. Moreover, by combining photopolymerization with flow polymerizations, i.e. photoflow, even more efficient polymerizations can be performed. In photoflow reactors, reaction mixtures are exposed to higher intensities leading to faster polymerizations. Furthermore, since reaction mixture are more homogenously irradiated, higher control of the polymerization can be achieved.[24]

1.4 Iniferter polymerization

Three main types of polymerization strategies show the controllable character of a CRP: nitrogen mediated polymerization (NMP)[25], atom transfer radical polymerization (ATRP)[26] and reversible addition-fragmentation chain transfer (RAFT)[27] polymerization. Requirements for control in these polymerizations are a fast initiation, extended lifetimes of growing chains and a low termination rate. For all three reaction mechanisms, these criteria are met by a same principle: there is a strict equilibrium between a dormant and an active state of the polymer. This equilibrium is achieved by either (i) reversible deactivation (for NMP and ATRP) or (ii) degenerative transfer (for RAFT). Activation of the dormant state allows the molecule to react with monomers and thereby induce chain propagation. Rapid deactivation provides equal probability for all chains to grow, which characterize the controllable behavior of these polymerization mechanisms. Consequences of CRP reactions are a constant propagation probability distributed over all chains, a linear increase of the number-average molar mass with monomer conversion, a low polydispersity and high end-group fidelity.[28] Thanks

to its versatility in reaction conditions, RAFT polymerizations can be defined as the most robust CRP reaction.

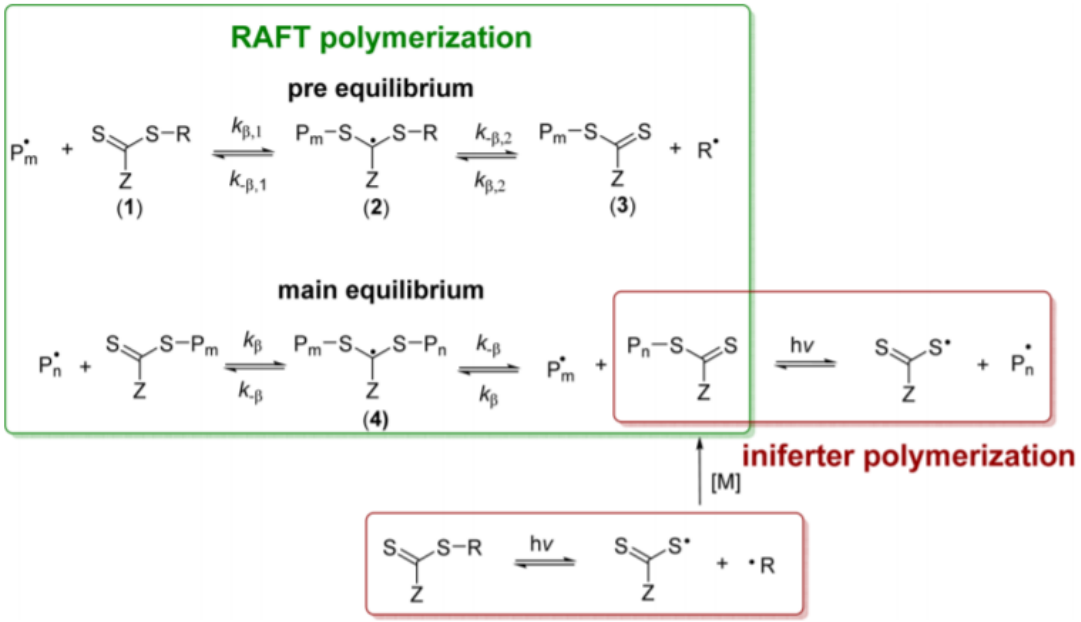

Figure 2 Reaction mechanism of both RAFT polymerization and iniferter polymerization. [24a]

The green box in figure 2 describes the mechanism of the RAFT polymerization. Thereby important is the requirement of a constant supply of radicals in the system for the complete time span of polymerization. Conventional radical initiators can fulfil this need. Upon energy absorbance, either by light or by heat, the initiator molecules fragmentate and radicals are generated. These highly reactive species can than attack the C=S bond of the RAFT-agent, mostly a trithiocarbonate, forming a radical intermediate. Due to the instability of this intermediate state, beta-scission follows and a new radical is generated. The system is now in its main equilibrium. The newly formed radical (R˙) can either react with a thiocarbonylthio group or with a monomer, initiating polymerization. Thanks to the fact that the rate of addition/fragmentation equilibrium is higher than the propagation rate, less than one monomer per activation cycle is added in the polymer chain. As a consequence, the degree of polymerization (DP) will be similar in all chains, resulting in the controlled behavior. When the radical source is depleted, different polymer species can be distinguished. A difference can be made on the ω-end of the polymer: with or without the thiocarbonylthio end-group, called living and dead chains, respectively. On the other hand, the nature of initiation defines the α-end: chains initiated by an initiator fragment and chains initiated by the RAFT agent R-group.[28a]

An interesting variant of this RAFT polymerization is the iniferter polymerization. Here, the constant supply of radicals is provided by the RAFT agent itself. UV or visible light triggers the fragmentation of the weak S-C bond adjacent to the C=S bond, resulting in a carbon-centered radical and sulfur-centered radical. The reactive carbon-centered radical can now react with a monomer or another RAFT-molecule. *Via* the first reaction, controlled chain propagation is provided by a reversible deactivation mechanism, whereas the latter reaction induces a degenerative chain transfer

mechanism like in conventional RAFT polymerizations. It should be stressed that no extra initiator molecules are needed for inducing polymerization. This leads to a big advantage in post-modification reactions onto surfaces, especially in the fabrication of block copolymers. Since polymerization in solution can be avoided in this way, the reinitiation, and thus the post-modification, is more straightforward.

In this master project, two compounds are explored as a possible RAFT agent for the 2PP application; A xanthate based RAFT-agent and a trithiocarbonate based RAFT-agent with an cyano-functionality (Figure 3). Sumerlin *et al.* already proved the success of xanthate iniferter polymerizations with N,N-dimethylacrylamide (DMA) as monomer.[29] Their work showed that, in comparison with the more conventional trithiocarbonate based RAFT-agents, xanthate based RAFT-agents have higher initiation rates. This is due to the difference in the mechanism of photolysis. Under mild UV light, photolysis in trithiocarbonate compounds results from the π-to-π* transition, whereas a spin forbidden n-to-π* transition led to photolysis in xanthates. The latter type of photolytic cleavage is known to be more rapid which explains the higher initiation rate of xanthates. It is believed that this property will be beneficial in the creation of block co-polymers in post-modification reactions. Besides the xanthate based RAFT-agent, also a classic trithiocarbonate is investigated in an iniferter mechanisms, as the these compounds are known for better controlling reactions.

The first objective of this thesis is the synthesis of methyl methacrylate (MMA) polymers in a controlled continuous flow polymerization. Poly(MMA) is chosen because of its robust nature (glass transition temperature of 110-120 °C)[30] which is believed to be optimal for the manufacturing of microstructures. Moreover, the material is biocompatible and is already widely used in biomedical applications, for instance for bone cement and eye implants.[31] Since reaction conditions are preferred to be similar to the Nanoscribe's setup in order to ensure possible reinitiation in 2PP and incorporation of the polymers into the final structures, polymerizations in an oxygen rich environment were investigated. UV-mediated polymerizations are of first-choice as this is the same wavelength range of the 2PP process.

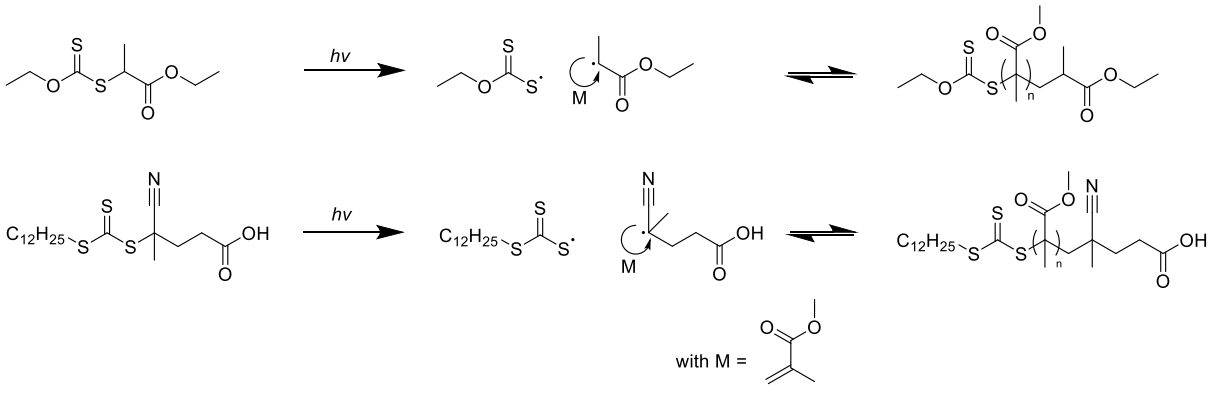

Figure 3 Reversible deactivation mechanism in iniferter polymerizations of the xanthate based RAFT-agent (top) and of the trithiocarbonate based RAFT-agent (bottom).

The synthesized polymers are then mixed with crosslinking monomers and a 2PA photoinitiator. Upon irradiation, the photoinitiator is fragmentated and might react with the polymers to induce polymerization *via* degenerative chain transfer. In this way, the polymer will be incorporated into the crosslinked structures. The obtained microstructures should have the end-groups of the RAFT-agents on the surfaces, which are available for further functionalization of the features. This can be achieved with an aminolysis on the carbon tail followed by a thiol-ene click reaction or covalent coupling of peptides on the acid end group *via* an esterification. Moreover, the reversible deactivation mechanism allows the synthesis of block copolymers which can be useful in specific applications. The Polymer Reaction Design (PRD) group has experience in both the aminolysis as well as the synthesis of block copolymers *via* RAFT/iniferter mechanisms.[32] Thanks to these chemical coupling reactions, growth factors, peptides or other chemicals can be attached to the final microstructures. In this way, both a topological control and a chemical control of cell behavior is targeted.

Chapter II – Materials and Methods

2.1 Materials

For the studies presented in the thesis, the following chemicals were used; 4,4'-azobis(4-cyanovaleric acid) (ACVA, Sigma-Aldrich, 98%), 2-bromo propionic acid (Acros 99%), carbon disulfide (Fisher, 99.9%), 2,2-dimethoxy-2-phenylacetophenone (DMPA, Acros, 99%), 1-dodecanethiol (TCI, 95%), ethyl 2-bromopropionate, hexylamine (Acros, 99%), IP-L (Nanoscribe GmbH), methyl methacrylate (MMA, stabilized, 99%), N,N'-dicyclohexylcarbodiimide (DCC, Acros, 99%), phenylbis(2,4,6-trimethylbenzoyl)phospine oxide (Irgacure 819, TCI, 95%), Poly(ethylene glycol) methyl ether acrylate (M_n=480, Aldrich), potassium ethyl xanthogenate, potassium hydroxide (Fisher, laboratory reagent gradient), p-toluenesulfonyl chloride (TCI, 99%), trimethylolpropane trimethacrylate stabilized with mequinol (MEHQ) (TRIM, TCI, 90%). All solvents used were obtained from commercial sources (Acros, VWR, Sigma-Aldrich) and used without further purification.

Cell culture components such as Minimum Essential Medium (α-MEM), fetal bovine serum (FBS) and penicillin-streptomycin were from Gibco, Life Technologies. Bovine serum albumin (BSA) and Triton X-100 were from Sigma-Aldrich. For fluorescence microscopy, the following probes were used: 4',6'-Diamidino-2-phenylindole dihydrochloride for nuclei (DAPI, Sigma-Aldrich), Alexa Fluor Phalloidin 647 for actin (Invitrogen™) and Calcein AM and EtD-1 (LIVE/DEAD™ viability/cytotoxicity kit, Invitrogen™).

2.2 Material Characterization

Polymer analysis

^{1}H-NMR spectra were recorded in CDCl3 on a Varian Inova 300 spectrometer at 300 MHz using a 5 mm probe.

Analytical SEC (Size Exclusion Chromatography) was performed on a Tosoh EcoSEC HLC-8320 GPC, comprising an autosampler, a PSS guard column SDV (50 x 7.5 mm), followed by three PSS SDV analytical linear XL (5 µm, 300 x 7.5 mm) columns thermostated at 40 °C (column molecular weight range: 1 x 10^2 –1 x 10^6 g·mol^{-1}), and a differential refractive index detector (Tosoh EcoSEC RI) using THF as the eluent at with a flow rate of 1 mL·min^{-1}. Toluene was used as a flow marker. Mark-Hawinks parameters were used for poly(MMA).[32c]

Electrospray ionization - mass spectroscopy (ESI-MS) was performed on an LTQ Orbitrap Velos Pro mass spectrometer (ThermoFischer Scientific) equipped with an atmospheric pressure ionization source 8 operating in the nebulizer-assisted electrospray mode. The instrument was calibrated in the m/z range 220-2000 using a standard solution containing caffeine; MRFA, and Ultramark 1621. A constant spray voltage of 5 kV was used, and nitrogen at a dimensionless auxiliary gas flow rate of 5 and a dimensionless sheath gas flow rate of 10 were applied. The S-lens RF level, the gate lens voltage, the front lens voltage and the capillary temperature were set to 50 %, -90 V, -8.5 V, and 275°C respectively. A 250 µL aliquot of polymer solution with a concentration of 10 µg·ml^{-1} was injected. A mixture of THF and methanol (THF:MeOH = 3:2), all HPLC grade, were used as solvent.

Infrared spectra were recorded using an attenuated total reflectance infrared (ATR-IR) from Bruker, tensor-27.

2PP Microstructures

Height profile measurements and 2D maps were acquired on a 3D laser scanning confocal microscope (Keyence VK-X250). The morphology of the microstructures were analyzed by scanning electron microscopy (SEM; FEI VERSA, Netherlands), coupled with elemental analysis performed by energy-dispersive X-ray spectroscopy (EDX; TEAM EDS system from EDAX, USA).[22]

2.3 Reactor setup

UV batch reactor

Glass vials containing the solution were placed on a stir plate in a Multilamp Reactor MLU 18 (12 × 15 W, λ_{max}= 254 nm) from Photochemical Reactor Ltd.

UV flow reactor

Fluorinated gastight PFA tubing was wrapped (reactor volume of 1 mL) around a UV fluorescent lamp (360nm) covered with aluminum foil. Reactor solutions were pumped into the reactor *via* a HPLC pump (Azura©, Knauer).

Blue-LED flow reactor

A custom-made tubular reactor cascade is built, consisting of fluorinated gastight PFA tubing (Advanced Polymer Tubing GmbH, 1/16'' OD, 0.75 mm ID, reactor volume of 1.1 mL), wrapped around a glass framework and placed in a silicon oil bath heated to 90 °C on an IKA RCT basic hot plate. Inside the glass framework 2 m of a blue light led strip (60 led/m, 450nm, 14.4W) from Ledsky is placed facing the PFA tubing. Reaction solutions are pumped into the reactor *via* a HPLC pump (Azura). (Adapted from [32c])

2.4 Syntheses

2.4.1 Reversible Addition Fragmentation chain Transfer (RAFT) Polymerization

Synthesis of ethyl 2-((ethoxycarbonothioyl)thio)propanoate (Xanthate RAFT)

The product was synthesized according to the literature procedure.[33] Ethyl 2-bromopropionate (4.08 g, 0.022 mol) and potassium ethyl xanthogenate (4.056 g, 0.011 mol) were dissolved in 40 mL ethanol. The solution was stirred under nitrogen for 4 hours in an ice bath. Afterwards, the solution was washed with 40 mL H_2O. The organic phase was extracted with 1:2 diethyl ether:pentane, dried over magnesium sulfate and filtered off. The solvent was removed under reduced pressure. ^{1}H NMR (400 MHz, cdcl3) δ 4.61 (q, J = 7.3, 0.8 Hz, 1H), 4.35 (q, 1H), 4.18 (q, J = 7.0, 0.8 Hz, 2H), 1.55 (d, J = 7.4 Hz, 3H), 1.39 (t, 3H), 1.29 – 1.24 (m, 3H).

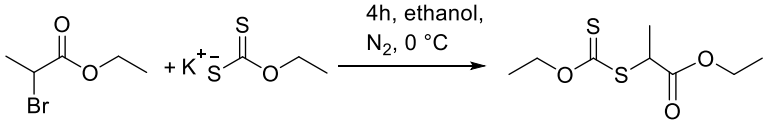

Scheme 1 Reaction scheme for the synthesis of *ethyl 2-((ethoxycarbonothioyl)thio)propanoate (Xanthtate RAFT)*

RAFT polymerization with ethyl 2-((ethoxycarbonothioyl)thio)propanoate (Xanthate RAFT-agent)

All reactions were performed with MMA as monomer.

Batch polymerizations

In a typical procedure, 7000 g·mol^{-1} (DP=68) was targeted as M_n. The reaction mixture was placed in a glass vial in the UV batch reactor. For the oxygen free reaction, the solution was purged for 5 minutes with nitrogen and the glass vial sealed with a septa. For the polymerization in the presence of oxygen, ambient air was allowed into the vial. ^{1}H NMR samples for conversion determination were taken at different time points to obtain the kinetic first-order plot.

Flow polymerizations

In a typical procedure, 7000 g·mol^{-1} (DP=68) was targeted as M_n. The solution was kept in a vial wrapped in aluminum foil in order to prevent possible light damage. The solution was pumped in the UV flow reactor (see 3.2 reactor setup). Different reaction times (residence times) were screened by changing the pump flow rates. Monomer conversions were determined *via* ^{1}H NMR (>95%). Molecular weight distributions were analyzed *via* GPC-SEC. End-group fidelity was analyzed *via* ESI-MS.

Synthesis of butane-1,4-diyl bis(2-((ethoxycarbonothioyl)thio)propanoate) (Bixanthate RAFT-agent)

2-bromo propionic acid (3.99 mL, 0.044 mol) and ethyl xanthic acid potassium salt (8 g, 0.05 mol) were dissolved in 80 mL ethanol and stirred for 4 hours under nitrogen. Subsequently, the organic phase was extracted with H_2O (3x) and brine (3x) and dried over magnesium sulfate. After evaporation of the solvents, 2-((ethoxycarbonothioyl)thio)propanoic acid) was obtained as a yellow oil. ^{1}H NMR (400 MHz, cdcl3) δ 4.68 (dd, J = 7.1, 1.6 Hz, 2H), 4.45 (q, J = 7.4 Hz, 1H), 1.63 (d, J = 7.5 Hz, 3H), 1.45 (t, J = 7.1 Hz, 3H).

Subsequently, 2-((ethoxycarbonothioyl)thio)propanoic acid) (5 g, 0.025 mol) and 1,4-butanediol (0.0773 g, 0.0008 mol) were dissolved in 7.5 mL DCM. The solution was stirred while being cooled on ice and a solution of DCC (0.531 g, 0.002 mol) and DMAP (0.0157 g, 0.0001 mol) in 2.5 mL DCM was dropwise added. The solution was stirred overnight at room temperature. The organic phase was collected and washed with H_2O (3x) and brine (3x). After drying over magnesium sulfate and removal of the solvents, butane-1,4-diyl bis(2-((ethoxycarbonothioyl)thio)propanoate) was obtained. ^{1}H NMR (400 MHz, cdcl3) δ 4.64 (q, J = 7.1 Hz, 4H), 4.39 (q, J = 7.4 Hz, 2H), 4.17 (d, J = 2.2 Hz, 4H), 1.78 – 1.71 (m, 4H), 1.58 (d, J = 7.4 Hz, 6H), 1.42 (t, J = 7.1 Hz, 6H).

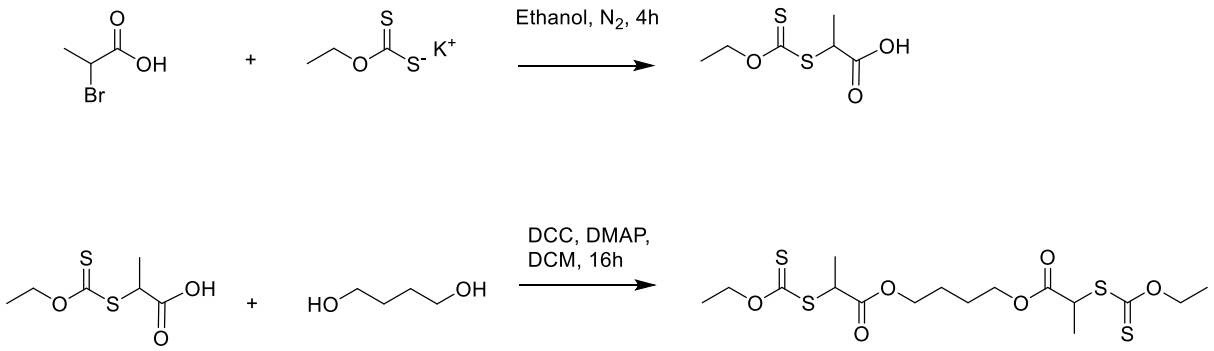

Scheme 2 Reaction scheme for the synthesis of *butane-1,4-diyl bis(2-((ethoxycarbonothioyl)thio)propanoate) (Bixanthate RAFT-agent).*

RAFT polymerization with bixanthate RAFT

MMA (1.07 mL, 0.01 mol) and the bixanthate RAFT (0.125 g, 0.0003 mol) were dissolved in 5 mL DSMO in a glass vial. The solution was purged with N_2 and placed in the UV batch reactor. ^{1}H NMR samples for conversion determination were taken at different time points to obtain the kinetic first-order plot.

Synthesis of 4-cyano4-[(dodecylsulfanylthiocarbonyl)sulfanyl]pentanoic acid (CDP RAFT)

1-Dodecanthiol (10.12 g, 0.05 mol) was dissolved in a 1:4 aceton:H_2O mixture and stirred on ice. KOH (3.366 g) was dissolved in 6.7 mL H_2O and subsequently dropwise added to the solution. Thereafter, CS_2 (3 mL, 0.05 mol) was added in one portion and the solution was stirred for 30 minutes at room temperature. After cooled down in an ice bath, p-toluenesulfonyl chloride (4.766 g, 0.025 mol) was added in one portion. Additionally stirring of 1 hour at room temperature and another 10 minutes at 45°C follows. After the precipitate was filtered with a glass filter, the product (bis(dodecylsulfanyl thiocarbonyl)disulfide was purified with flash column chromatography (85:15 hexane:DCM).

The final product was synthesized according to literature.[34] (Bis(dodecylsulfanyl thiocarbonyl)disulfide (9.3943 g, 0.016 mol) and 4,4'-azobis(4-cyanopentanoic acid) (7.115 g, 0.025 mol) were dissolved in ethyl acetate and overnight stirred under reflux at 80°C. In the morning, an additional portion of 4,4'-azobis(4-cyanopentanoic acid) (2.371 g, 0.008 mol) was dissolved in ethyl acetate and added to the solution which was stirred for another hour at 100°C. After removal of the solvent under lower pressure, the product was purified with gradient column chromatography (100 hexane to 34:66 ethyl acetate/hexane). After removal of the solvents, the product was obtained (10.3737 g, 0.026 mol). Yield=80% ^{1}H NMR (400 MHz, cdcl3) δ 3.35 – 3.31 (m, 2H), 2.73 – 2.63 (m, 2H), 1.89 (s, 3H), 1.74 – 1.65 (m, 2H), 1.47 – 1.20 (m, 18H), 0.87 (t, 3H).

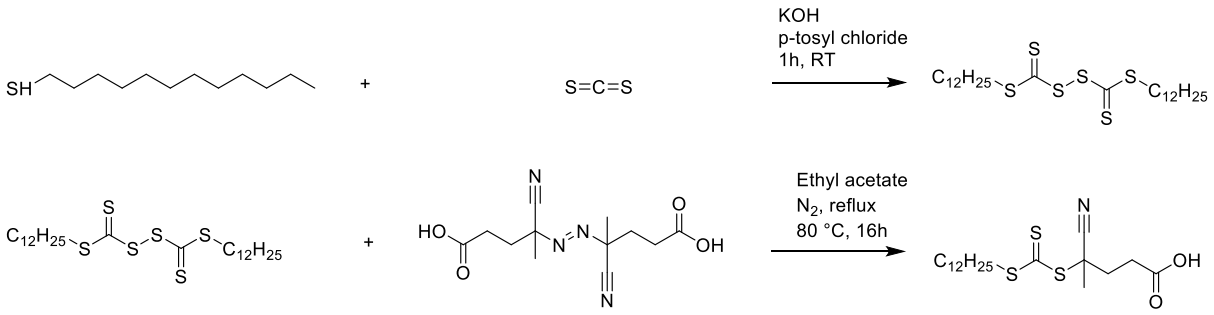

Scheme 3 Reaction scheme for the synthesis of 4-cyano4-[(dodecylsulfanylthiocarbonyl)sulfanyl]pentanoic acid (CDP RAFT-agent)

RAFT polymerization 4-cyano4-[(dodecylsulfanylthiocarbonyl)sulfanyl]pentanoic acid (CDP RAFT)

In a typical procedure, 5000 g·mol^{-1} (DP=46) was targeted as M_n. Different concentrations of MMA were tested (0.5M, 1M, 1.5M, 2M). The solution of MMA and xanthate RAFT-agent was kept in a vial wrapped in aluminum foil in order to prevent possible light damage. For the UV-mediated polymerizations, the same setup was used as the xanthate flow polymerizations. For the blue light mediated polymerizations, the reaction mixture was purged with nitrogen for 5 minutes prior to being pumped into the blue-LED flow reactor. Different reaction times (residence times) were screened by changing the pump flow rates. Monomer conversions were determined *via* ^{1}H NMR (>95%). Molecular weight distributions were analyzed *via* GPC-SEC. End-group fidelity was analyzed *via* ESI-MS.

2.4.2 Resin Composition and Optimization

Exact masses were calculated based on mol%, where the total mol was the sum of the amount mol of crosslinker (always 0.4 mL) , photoinitiator and polymer. DMSO was added in volumetric portions to increase solubility. Prior the 2PP, resin were tested under a XeF excimer laser (λ = 351 nm, 4 – 6 ns pulses, 1.5 mJ per pulse). One droplet of the resin was placed onto a glass microscope substrate. Laser shots were fired with a frequency of 100Hz and a power of 1.5 mJ.

2.4.3 Fabrication of Microstructures with Two-Photon Polymerization

Parameter test are performed in piezo scan mode to optimize laser power and scan speed. Five lines with increasing height (from 0.5 µm to 2.5 µm; length 10 µm) and spacing of 0.5 µm was seen as one unit. In the x-axis, 5 units were printed with increasing laser power (100%=50mW). For each laser power, 5 units were printed in the y-axis, each with different scan speeds. In this way, 25 distinct laser power-scan speed combinations could be screened in one print (Figure S1). First line observations were done with the optical microscope of the Nanoscribe. Further analysis were done with the profilometer, SEM and EDX. After defining the optimal laser parameters, cross arrays are printed.

Drawings of the objects for 2PP printing were made using Solidworks (Dassault Systèmes) and the files were saved in STL formats. Fabrication of 3D microstructures was performed with a 3D laser lithography system (Nanoscribe GmbH, Photonic Professional). Conversion into machine language was done using the proprietary software belonging to the equipment manufacturer. The excitation source was a Ti-Sapphire femtosecond (fs) laser with a wavelength of 780 nm, emitting 150 fs pulses at 100 MHz and 50 mW at sample surface. The laser beam was focused within the resin using a 63× microscope objective with a numerical aperture of 0.75. A resin drop was placed on top of a 0.17 mm glass cover slide, and positioned in the sample holder. After exposure, development was done using PGMEA during 5 to 10 minutes, followed with isopropanol (IPA) and drying using gentle nitrogen blow (adapted from [22]).

2.3.4 Post-modification of the Polymers

The resins were smeared over a glass substrate in order to obtain a smoother surface rather than a droplet. Subsequently, UV irradiation with the excimer laser (1.5mJ, 100Hz, 15 seconds) crosslinked the resin. The disc of crosslinked polymer was placed in a glass petri dish. Unreacted resin was removed with THF (2 times). A solution of hexylamine (1 eq.), PEG-acrylate (2 eq. ; 480 g·mol^{-1}) and THF was added to the polymer disc. The petri dish, covered in aluminum foil, was placed onto a shaking plate for 2 hours. Thereafter, the mixture was removed and the disc was washed again with THF (2 times), isopropanol and dried under gentle N_2 flow.

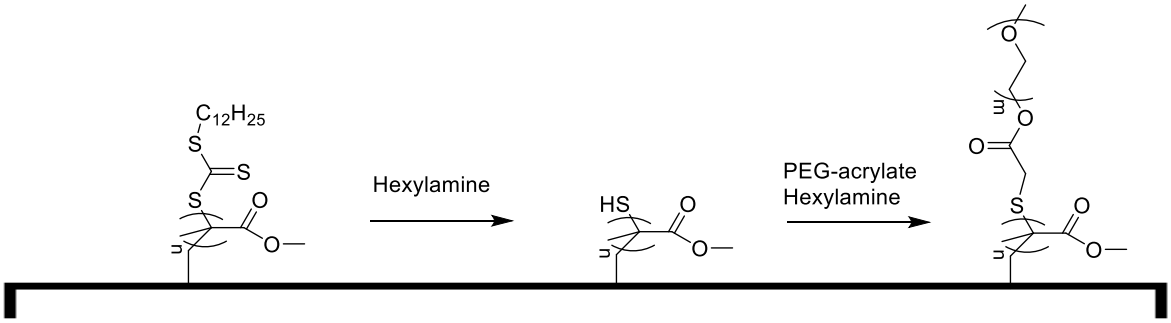

Scheme 4 Reaction scheme of post-modification reaction of the crosslinked structures.

2.5 Cell Experiments

Cell culture

Human osteosarcoma MG-63 cells were cultured in alpha minimum essential medium (α-MEM) supplemented with 10 % fetal bovine serum (FBS), 1 % penicillin-streptomycin, 1 % glutamine, 1 % HEPES and 1 % sodium pyruvate. The cells were cultured at 37 °C in a humidified atmosphere of 5 % CO_2. Medium was replaced every 2 to 3 days. Cells were sub-cultured in standard culture flasks upon reaching 80-90 % confluence, and then trypsinized with 0.25 % trypsin/EDTA for 5 minutes at 37°C. Trypsin was inactivated with three times its volume in medium, and used for experiments or sub-cultured (from [22]).

Fluorescence staining and imaging

Prior to cell seeding, the substrates were washed twice in 70 % ethanol for 5 minutes and twice in sterile phosphate buffered saline (PBS) for 5 minutes. Cell were seeded onto the substrates with the microstructures inside 6-well plates at a density of 10 000 or 20 000 cells/cm^2, in a working volume of 3 mL cell culture medium per well (adapted from [22]).

Seeded cells were visualized under brightfield and phase contrast microscopy (Nikon TS100) for first line quality control and live assessment of the cells.

Cell viability was further analyzed with the Live/Dead assay from Invitrogen. 10 µL of 2mM EtD-1 and 2.5 µL of Calcein AM was added to 10 mL sterile PBS and mixed. 3mL of the solution was added to the 6-well plates containing the substrates with the microstructures. Subsequently, the cells were incubated for 45 minutes. Thereafter, the mixture was replaced by sterile PBS. Visualization was performed with fluorescence microscopy (Nikon Ti-Eclipse).

Cell attachment and morphology were evaluated by a two-channel fluorescence imaging of the nucleus and F-actin. Upon culture for one day, the medium was removed and the samples were washed with PBS and fixed with 4 % paraformaldehyde for 20 minutes at room temperature. For fluorescent staining, samples were washed twice with 0.1 % Tween-20 in PBS, permeabilized with 0.1 % Triton X-100 in PBS for 5 minutes, and washed twice with 0.1 % Tween20 in PBS (PBST). Thereafter, the samples were incubated in Phalloidin-647 (1:100 in PBST) for 45 minutes, washed with PBST and again incubated in DAPI solution (1:100 in PBST) for 10 minutes. After washing with PBST, the samples were stored in PBST at -20 °C (adapted from [22]). The fixated cells were visualized with fluorescence microscopy (Nikon Ti-Eclipse).

Chapter III – Results and Discussion

3.1 Synthesis of Iniferter Polymers

3.1.1 Xanthate RAFT-agent Polymerizations

Firstly, a xanthate based RAFT-agent was used in an iniferter mechanism. Eventually, these polymers could be mixed in 2PP resins to allow post-modification *via* the end-groups of the polymers. The synthesis of the polymers will be performed with UV-light since it mimics the 2PP process. This allows the initial testing of end-groups preservation under UV irradiation, which is important for the post-modification reactions. A noteworthy difference with conventionally controlled radical polymerizations is the fact that the Nanoscribe's setup requires processing in an oxygen-rich environment. Such condition can be challenging since O_2 molecules can disturb radical reactions by quenching.[35] First investigations were therefore based on an oxygen tolerant polymerization. Two batch polymerizations with the same reaction conditions ($M_{n,target}$=5000 g·mol^{-1}, 2M MMA) were performed. As solvent, DMSO was chosen as it is known as an excellent solvent for photoiniferter reactions. One reaction mixture was purged with nitrogen for 5 minutes prior to UV-light exposure, whereas the second was polymerized in a vial open to atmosphere. At different time points, samples were collected and analyzed with ^{1}H NMR in order to acquire kinetic first-order plots (Figure 4). Almost complete overlay of the two curves was observed. After 60 minutes of polymerization, both reactions reached a monomer conversion of 75%. For the sample open to the atmosphere, the monomer could partially be evaporated, which means the monomer conversion could be an overestimation and should be taken with caution. Nevertheless, a complete overlay indicates that there was probably no significant difference in monomer consumption for polymerizations in an oxygen environment compared to polymerizations in an oxygen-free environment.

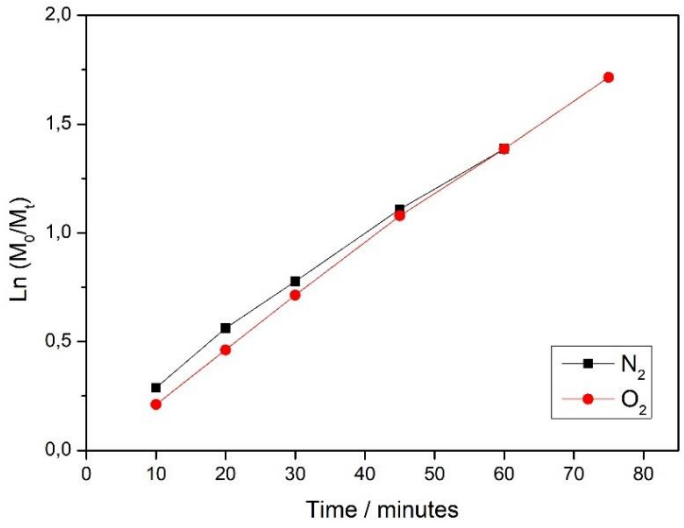

Figure 4 Comparison of kinetic first-order plots of pMMA polymerized in an oxygen environment with pMMA polymerized in a nitrogen environment. Reaction conditions were the same for both polymerization reactions ($M_{n,target}$=5000 g·mol^{-1}, 2M MMA, DMSO, UV batch reactor).

In order to improve the reproducibility and to facilitate up-scaling of the procedure, a photo-flow polymerization was explored. Based on previous results of the polymerization being sufficiently oxygen tolerant in a batch setup, reaction mixtures were not purged with nitrogen before exposure to UV-light. To get better insights into the kinetics of the polymerization, different reactions were performed each with another concentration of MMA (0.5M, 1M, 1.5M, 2M). Again, the kinetics of each polymerization were monitored by taking ^{1}H NMR samples at different time points. For all the kinetic first-order plots, two phases can be distinguished (Figure 5). Firstly, for low residence times, a linear trend between residence time and $Ln(M_0/M_t)$ was observed. For residence times higher than approximately 5 minutes, the monomer conversion remained constant. This 5 minutes residence time corresponded to 26%, 42%, 45% and 48% monomer conversion for monomer concentrations of 0.5M, 1M, 1.5M and 2M, respectively. The plateau phase is situated at higher $Ln(M_0/M_t)$ values as the monomer concentration increases. The linearity seen in low residence times indicates a constant concentration of propagating chains, whereby the steepness of the slope relates to the propagation constant k_p. As expected, at higher monomer concentrations, the slopes becomes steeper. This can be explained by the fact that the chance of a reaction between a propagating chain and a monomer is higher when there are more monomer units in solution i.e. at higher concentrations. Although the linearity is a requirement for obtaining a controlled radical polymerization, it does not directly imply a controlled behavior. The linearity can be a result of a balance in initiation and termination rates (as in conventional radical polymerizations) rather than an equilibrium between activation/deactivation. A contradiction of a fully controlled polymerization that can be derived from the kinetic first-order plots, is the plateau phase. Such trend is typical for termination.

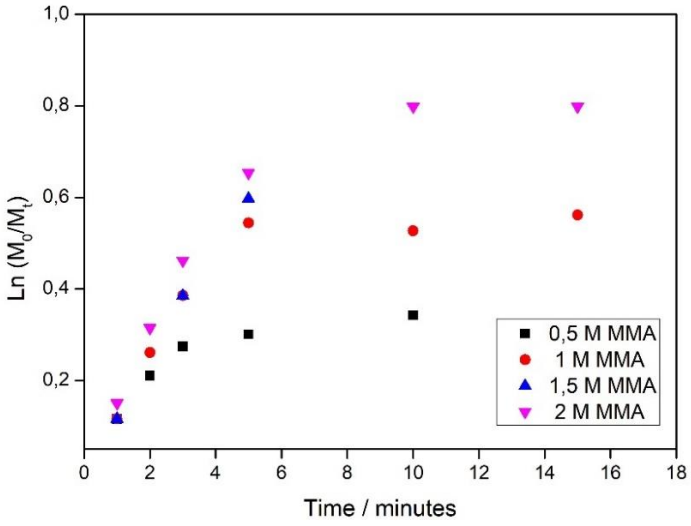

Figure 5 Kinetic first-order plots of xanthate RAFT-pMMA synthesized with different MMA concentration (0.5M, 1M, 1.5M, 2M). Reaction mixtures were not purged with nitrogen. All polymerizations were performed in same conditions ($M_{n,target}$=7000 g·mol^{-1}, DMSO as solvent, UV-flow setup).

Interesting to notice is that this behavior was not seen in polymerizations in solution, indicating that this problem is probably partially due to the reaction conditions. In general, light intensities in flow reactors are higher compared to batch reactors leading too more efficient radical formation. This higher concentration of radicals will eventually lead to higher termination rates. By performing the reaction in milder conditions, i.e. lower light intensities, radical concentration might become lower and termination reaction could be suppressed in this way. Longer reaction times are the drawback of this solution.

In the previous experiments, DMSO was used as solvent. Because DMSO is relatively difficult to handle, other solvents were explored. To this end, the same reaction ($M_{n,target}$= 3000 g·mol^{-1}, oxygen environment, 2M MMA, UV-flow setup) was performed in three different solvents; DMSO, butyl acetate and dioxane. The propagation constant of both butyl acetate and dioxane is significant lower than the propagation constant of DMSO. This lower efficiency of dioxane and butyl acetate was also suggested by the lower conversions after 15 minutes: 80%, 53% and 52% for DMSO, butyl acetate and dioxane, respectively. Despite the lower efficiency of polymerization, further reactions were done in butyl acetate or dioxane, because the solvent could be evaporated overnight under reduced pressure, obtaining pure polymer already the day after synthesis.

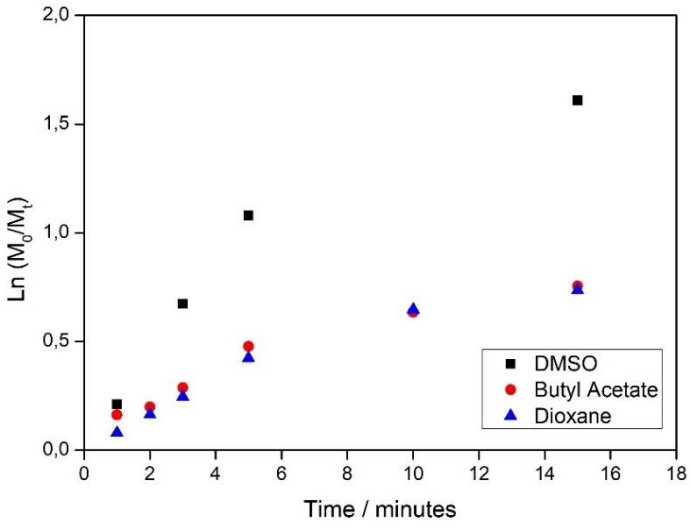

Figure 6 Kinetic first-order plots of xanthate RAFT-pMMA in DMSO, butyl acetate and dioxane. All polymerizations were performed in same conditions ($M_{n,target}$=3000 g·mol^{-1} 2M MMA, oxygen environment, UV-flow setup).

In order to further analyze the kinetic behavior of the xanthate photoiniferter mechanism, molecular weight distributions were obtained *via* GPC. Samples of different residence times were taken from a xanthate photoinferter polymerization in flow. The targeted molecular weight ($M_{n,target}$) was 3000 g·mol^{-1} with a monomer concentration of 2M MMA. Here, butyl acetate was used as the solvent. The molecular weight distributions exhited bimodal distributions (Figure 7). The first peaks were observed at around 200 g·mol^{-1} and can be assigned to unreacted xanthate RAFT-agent (M_n = 222.04 g·mol^{-1}). The intensity of the peak decreases with increasing residence times. The second peaks are dedicated to the polymer distributions as these show increasing molecular weights with increasing residence times i.e. monomer conversion. It should be noted that M_n and $Đ$ values

do not provide reliable information about the polymers because of this bimodal distribution. Nevertheless, it was shown that the first peak was almost non-excisting in the GPC trace of the 10 minutes residence time, making it possible to determine the M_n and $Đ$ values. The 10 minutes residence time corresponded to a conversion of 47% according to ^{1}H NMR analysis. The GPC measurements for the same sample showed a M_n value of 892 g·mol^{-1} and a Đ value of 1.81.

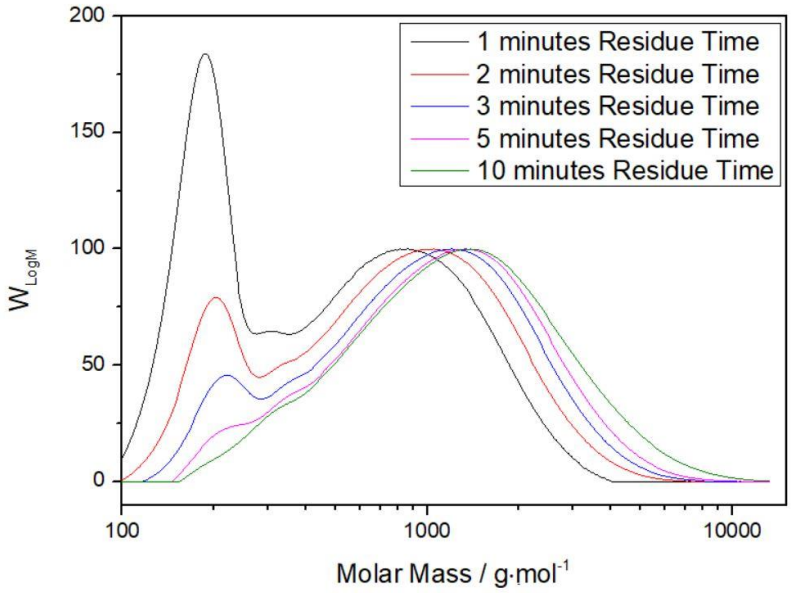

Figure 7 Overlay of GPC molecular weight distributions of a xanthate RAFT-pMMA after different residence times. ($M_{n,target}$=3000 g·mol^{-1} 2M MMA, butyl acetate as solvent, oxygen environment, UV-flow setup). The first peaks can be assigned to the unreacted xanthate RAFT whereas the second peaks are polymer distributions.

By combining molecular weight distributions derived from GPC and the kinetic first-order plots a possible explanation for the monomer conversion stop can be given. As is seen in the kinetic first-order plot, the plateau phase started at around 5 minutes residence time. At about the same time point, the peak dedicated to the xanthate RAFT agent had almost completley disappeared. It is therefore most likely that this depletion of xanthate RAFT-agent is linked with termination seen in ^{1}H NMR. When trying to explain that precise time point of depletion i.e. 5 minutes residence time, it is important to study the half-life time of the xanthate RAFT-agent in UV-light. It is plausible that, at this particular time, the xanthate RAFT-agent is destroyed which makes it unable to further polymerize. The exact polymerization mechanism and reason for the termination cannot be concluded with high certainties using these data. But at least it can be concluded that no control was obtained in this iniferter polymerization since an unwanted termination reaction occured. This is also confirmed by the high $Đ$ value (1.81) of the 10-minute sample.

For a complete end-group analysis of the polymers, ESI-MS spectra were measured. The same polymers as with the previously discussed GPC date were measured ($M_{n,target}$=3000 g·mol^{-1} 2M MMA, butyl acetate as solvent, oxygen environment, UV flow setup). Two distribution can be distinguished on the ESI-MS spectra (Figure 8). The smallest distribution can be assigned to the xanthate RAFT-MMA polymers. The larger distribution is dedicated to the xanthate RAFT-MMA polymer distribution without the xanthate end-group. These findings indicate relatively low end-group fidelity.

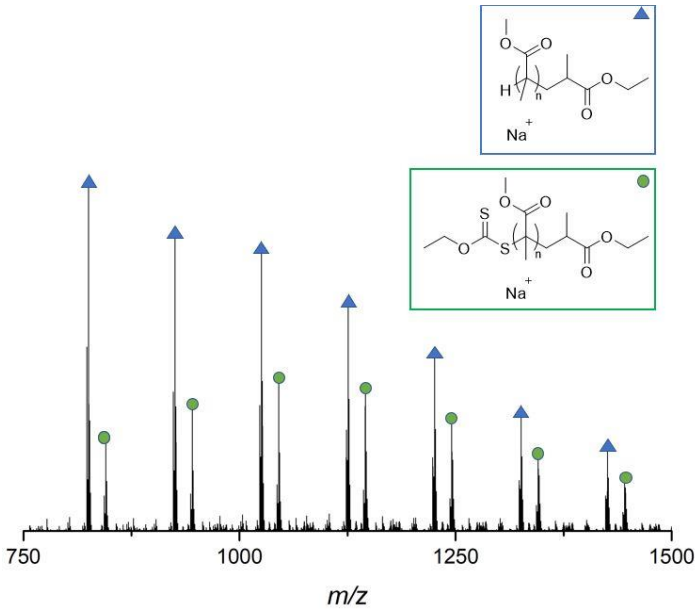

Figure 8 ESI-MS spectra of xanthate RAFT-pMMA in butyl acetate. ($M_{n,target}$=3000 g·mol^{-1} 2M MMA, butyl acetate as solvent, oxygen environment, UV-flow setup). The smallest distribution is assigned to polymers with both original RAFT-end groups in their structures whereas the larger distribution is assigned to polymers without the xanthate end-group.

It is hypothesized that incorporation of polymers with two RAFT end-groups in a 2PP resin can lead to more accessible end-groups on the surfaces of microstructures allowing a more efficient post-modification. Therefore, two single RAFT agent were coupled together *via* a DCC coupling and examined in an iniferter polymerization. However, first experiments in the UV-batch reactor in an oxygen free environment already displayed end-group loss in ESI-MS (Figure 9). Surprisingly, the main distribution is dedicated to the polymer species with only one original RAFT end-group.

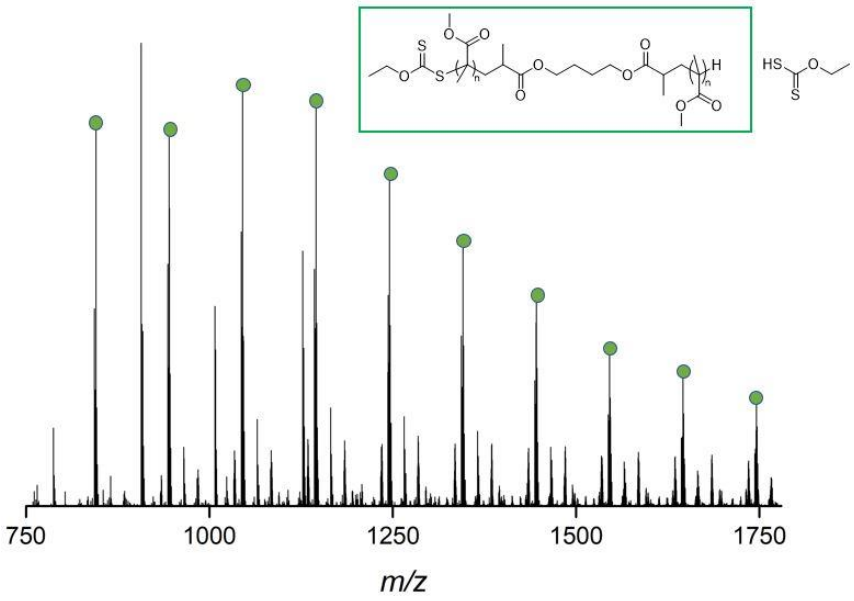

Figure 9 ESI-MS spectra of bixanthate RAFT-pMMA made in DMSO. ($M_{n,target}$=4000 g·mol^{-1} 2M MMA, oxygen-free environment, UV-batch reactor) The distribution is assigned to pMMA with only one RAFT end-group.

In this section, a xanthate RAFT was investigated for the incorporation into a 2PP resin. It was hypothesized that the high initiation rate of these molecules would lead to a higher efficiency in 2PP and thereby a high end-group concentration onto the surfaces of microstructures. Although polymerization under UV-light and in an oxygen environment occurred, the controllable character was not observed. Furthermore, loss of RAFT end-groups was observed, making the post-modifications of the polymers inefficient. While the xanthate RAFT-agent did not seem to polymerize in a controlled way for MMA, literature demonstrated effective and fast polymerizations with other monomers.[29, 36] Therefore, monomers, such as vinyl acetate[37], may be investigated in the future, to obtain a better retention of the end-groups. In this thesis, we chose, however, to work further with pMMA since it is hypothesized that the robust nature could be interesting for printing microstructures and cell experiments.

3.1.2 CDP RAFT-agent Polymerizations

Since the xanthate RAFT did not display a controlled polymerization, a conventional trithiocarbonate (4-cyano4-[(dodecylsulfanylthiocarbonyl)sulfanyl]pentanoic acid (CDP)) was tested in an iniferter polymerization. To get insights in the kinetic behavior of the polymerization, a BiCDP was not directly investigated. If the polymerization is successful, a BiCDP can be polymerized to increase the amount of end-groups and eventually the efficiency of post-modification reaction onto surfaces of crosslinked structures. Previous work in our group already showed successful iniferter polymerization in an oxygen-free environment under blue light using MMA as monomer. These reaction showed linear M_n-conversion plots and Đ values of 1.3.[32c]. To mimic the 2PP setup, polymerizations were tested in an oxygen rich environment and under UV light.

The M_n -conversion plot showed a linear relationship until 40% monomer conversion. Average molecular weights values of conversions higher than 40% did not show the expected linearity of a controlled polymerization (Figure 11). Moreover, increasing Đ values up to 2.27 confirms the loss in control of the reaction with higher conversion. It is likely that the UV-light is too harsh for the reaction and destroys the RAFT-agent or induces side-reactions. UV-induced damage of the RAFT-agent was also reported by Quin *et al*.. [38] Their work demonstrated broadening of the molecular weight distribution for pMMA polymerization reactions with relatively long exposure times (>48h in batch reactions) to UV-light, i.e. conversion of 30%. Studies with another RAFT-agent and acrylic acid as monomer showed a controlled polymerization using UV with conversions up to 50% in 5.5 h.[39] These findings indicate that the UV-induced damage is linked with the type of RAFT-agent and could probably be reduced when using other systems.

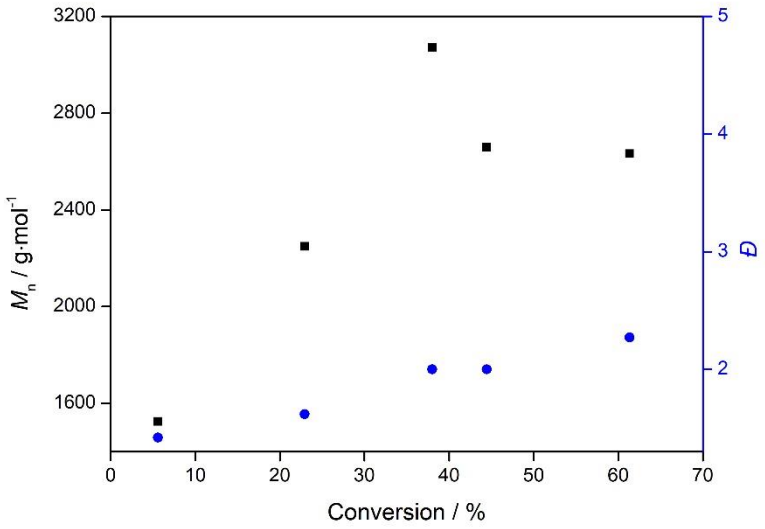

Figure 11 Conversion-M_n plot and polydispersity of CDP RAFT-pMMA ($M_{n,target}$ =5000 g·mol^{-1}, 8M MMA, dioxane, oxygen environment, UV-flow reactor). Loss in linearity with higher conversion and relatively high Đ values (up to 2.27) suggest failure in control of the iniferter polymerization.

Also for these polymers, end-group fidelity was examined with ESI-MS analysis (Figure 12). The most pronounced distribution was assigned to the polymers with both original RAFT end-groups. It should be noted that, for this distribution, one polymer molecule is coupled to two Na^+ ions, one from conventional ionization for mass detection in the orbitrap and a second from the exchange with the proton from the carboxyl group of the polymer. Despite the presence of the expected polymer distribution, many side products were observed. These were probably a result of the destruction of the RAFT end-groups or unusual side reactions. These findings confirms the non-linearity of the M_n-conversion plot and the high Đ values measured with GPC.

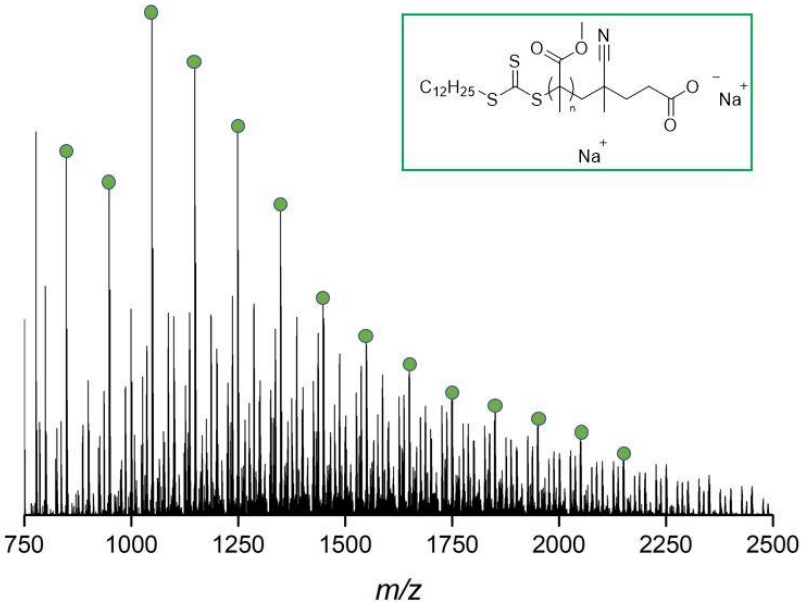

Figure 12 ESI-MS spectrum of CDP RAFT-pMMA ($M_{n,target}$=5000 g·mol-1, 8M MMA, dioxane, oxygen environment, UV-flow reactor). The distribution is assigned to the CDP RAFT-pMMA. Smaller peaks are side products of the polymerization.

Taken together the M_n-conversion plot and ESI-MS analyses, it was shown that it was not possible to achieve high control over this iniferter polymerization. A non-linear M_n-conversion correlation and high polydispersity with higher conversions (>40%) contradicts a fully controlled radical polymerization. Also, ESI-MS showed the presence of side products, indicating low end-group fidelity.

Both a control in polymerization and high end-group fidelity are important for incorporating the polymers into a 2PP resin. Iniferter polymerization of the CDP RAFT-agent under UV-light did not fulfill these requirements. However, since polymerization did occur and polymers with both RAFT end-groups were present in reactions with low conversion according to ESI-MS, it can be expected that in 2PP the intact RAFT groups will be involved in the polymerization reaction. Therefore, the CDP polymers could be incorporated into the structures. Nevertheless, achieving a high end-group fidelity before being subjected to 2PP was preferred. Therefore, another strategy was exploited. As already mentioned, previous work in our group successfully synthesized well-controlled CDP-MMA polymers. These reaction were performed in a flow setup under blue LED in an oxygen-free environment.[32c] Since blue light does not mimic the 2PP setup anyway, polymers were synthesized as described.

The linear correlation of the M_n-conversion plot indicates a controlled radical polymerization in blue light (Figure 13). Moreover, the polydispersity, measured with GPC, was almost constant at around 1.3, which is acceptable for a CRP. These values are in line with other polymerizations described in literature.[32c, 40]

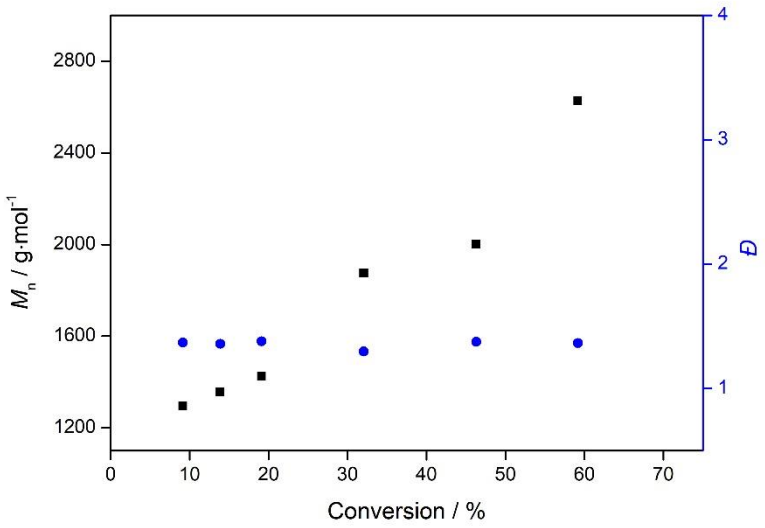

Figure 13 Conversion-M_n plot and polydispersity of a CDP-pMMA synthesized in blue light ($M_{n,target}$=5000 g·mol^{-1}, 8M MMA, dioxane, oxygen environment, blue-LED flow reactor). The linearity and the constant Đ values (around 1.3) indicates a controlled behavior of the CDP iniferter mechanism in blue light.

Despite the higher control of polymerizations in blue light over UV-light, kinetic first-order plots showed a slower propagation rate in blue light mediated polymerization (Figure 14). This could also be concluded from the conversion at 10 minutes residence time; 22% and 9% for UV light and blue light, respectively. It has to be noticed that the comparison of higher residence times gives no reliable information about the propagation rate since conversion of UV light mediated polymerizations exceeds 40%, meaning loss of control. Furthermore, a short inhibition time (< 5 minutes) was observed for both the polymerization in blue light and UV light.

McKenzie *et al.* performed similar iniferter reactions with a tritiocarbonate in the two wavelength ranges.[41] Their work showed also the short inhibition time, however, longer in blue light mediated polymerization. Also, slope steepness of the kinetic first-order plot were almost identical for both reactions. These findings were, however, not observed in our experiments. This might be because of the different reaction conditions of the two polymerizations and the fact that McKenzie *et al.*

performed the reactions in solution, yielding different reaction mechanisms. Further experiments in identical reaction conditions could clarify this behavior.

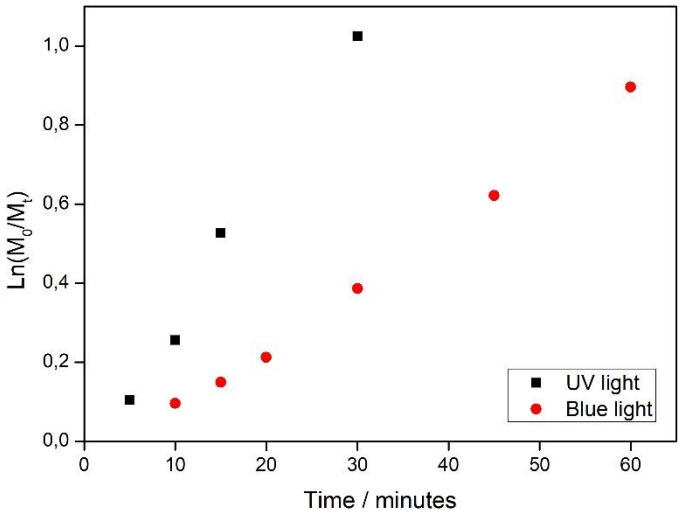

Figure 54 Comparison of kinetic first-order plots from CDP-pMMA synthesized in UV light ($M_{n,target}$=5000 g·mol^{-1}, 8M MMA, dioxane, oxygen environment, UV flow reactor) and CDP-pMMA synthesized in blue light ($M_{n,target}$=5000 g·mol^{-1}, 8M MMA, dioxane, oxygen free environment, blue-LED flow reactor).

By comparing the ESI-MS output of the blue light polymerization with the UV light polymerization (Figure 15 versus Figure 12, respectively) , a clear difference was seen. In blue light, the only distinct distribution can be assigned to the CDP polymers. Whereas the polymers synthesized in UV light had two sodium ions per molecule, the polymers produced by using blue light only had one, meaning that no ion exchange occurs with the proton of the carboxyl group

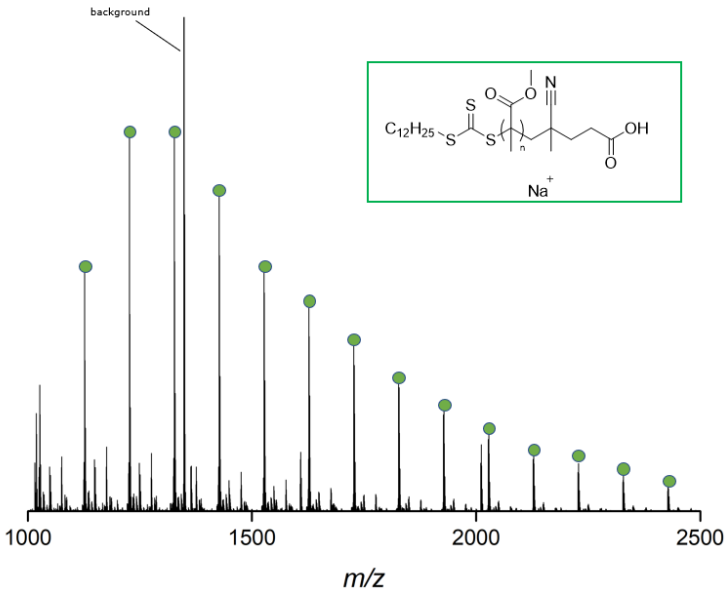

Figure 15 ESI-MS spectrum of CDP-pMMA synthesized in blue light ($M_{n,target}$=5000 g·mol-1, 8M MMA, dioxane, oxygen environment, blue-LED flow reactor). The distribution is assigned to CDP-pMMA.

To conclude this section, the synthesis of two RAFT polymers was examined in iniferter polymerization. In order to develop polymers that can be used in 2PP, reactions conditions for the synthesis were similar to the 2PP setup, i.e. oxygen rich environment and UV-light. Both the xanthate RAFT-agent and the CDP RAFT-agent showed loss in control of polymerization in such conditions according to ^{1}H NMR and GPC analyses. Also, a relatively low end-group fidelity was observed with ESI-MS analysis. Therefore, polymerizations with the CDP RAFT-agent were examined under blue LED-light as described in literature. For these pMMA polymers, the three criteria for defining a CRP were met: i) a linear M_n-conversion plot, ii) polydispersity values between 1.0 and 1.5 and iii) high end-group fidelity in ESI-MS. By incorporating these polymers into a 2PP resin, RAFT end-groups on the surface of the microstructures might be accessible for post-modification reactions.

3.2 Photocurable Resin for 2PP

In this section, the composition of a photocurable resin will be described. Although the resin was especially designed for 2PP, first-line experiments were performed with conventional UV-laser polymerization. As reference, commercial resin were crosslinked under the UV-laser. Time points of hardening of a droplet were 30 seconds, 50 seconds and 1 minutes for the IP-L, IP-DIP and IP-S, respectively. Resin which hardens under the UV-laser before 30 seconds were tested in 2PP. It is important to keep in mind that one-photon absorption is a different process as two-photon absorption, so successful polymerization under a UV-laser does not directly imply success in a 2PP setup. This is clearly demonstrated by the choice of photoinitiator later in this section.

Table 1 Overview of the commercial resins from Nanoscribe with their time point of hardening under the UV-laser.

Resin	Time point of hardening
IP-L	30 seconds
IP-DIP	50 seconds
IP-S	1 minute

A photocurable resin consists of at least two components; a crosslinking monomer and a photoinitiator. Herein, we report a resin with a third ingredient, namely a polymer synthesized *via* an iniferter polymerization. Thanks to these molecules, post-modification onto the crosslinked microstructures should be possible either *via* addition of a polymer block or *via* chemically coupling onto the end-groups. Next paragraphs discuss each component of the resin in more detail.

Crosslinking monomer. As crosslinking monomer, two molecules were taken into consideration to use in a 2PP resin: Tetra(ethylene glycol) diacrylate (TEGDA) and trimethylolpropane trimethacrylate (TRIM), a diacrylate and a trimethacrylate (Figure 15). In both crosslinkers, 5 mol% photoinitiator (i.e. DMPA) was dissolved in 0.4 mL crosslinker. Both resins solidified after 10 seconds under the excimer laser. Despite literature suggest the use of acrylic crosslinkers because of their fast polymerization kinetics, further experiments were done with TRIM, a methacrylate.[18] Due to the fact that TRIM has one vinyl group more than TEGDA, it was hypothesized that TRIM gives more dense crosslinked microstructures. Moreover, the glass transition temperature for methacrylic monomers is in general higher than for acrylic monomers, leading to more robust structures.[42] TRIM is probably also more compatible with the MMA polymers that will be added to the resin.

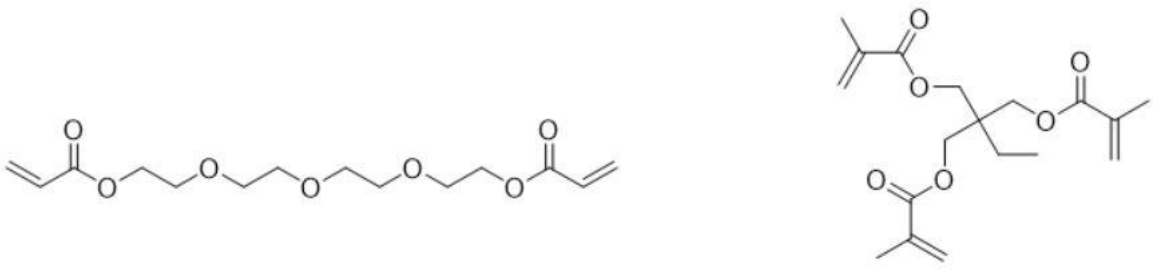

Figure 16 Chemical structures of Tetra(ethylene glycol) diacrylate (TEGDA) (left) and trimethylolpropane trimethacrylate (TRIM) (right)

Photoinitiator. In the previous section, it was already shown that the CDP polymer dissociates under UV-light and thereby can act as an initiator. With this in mind, first experiments were performed without an additional photoinitiator. However, crosslinking of a resin containing only TRIM and CDP polymer under the UV-laser was not successful. This result was somehow excepted since the RAFT agent don't meet the 2PA photoinitiator criteria given by literature.[20] This implies that an additional photoinitiator must be added to induce crosslinking. When irradiated, these molecules generate radicals which can activate the degenerative chain transfer mechanism of the polymers. In this way, the polymers can be incorporated into the crosslinked microstructures. Although the 2PP photoinitiator in Nanoscribe's IP-L resin is very effective, the high cost of the molecule was a reason to explore different photoinitiators (Figure 16).

The first molecule in analysis was 2,2-dimethoxy-2-phenylacetophenone (DMPA), which is a classical UV initiator. Upon energy absorbance, bond breaking occurs leading to radical generation. DMPA is known as an efficient photoinitiator for linear photon absorption experiments.[43] Secondly, Irgacure 819 was examined as a potential 2PP photoinitiator. Despite the relatively low σ value of the molecule i.e. 5 GM measured by Hagan *et al*. [44], this centrosymmetric molecule meets the requirements of effective 2PA. The two 1,3,5-trimethylbenzene end-groups and the double bond oxygen onto the phosphor act as electron-donors and an electron-acceptor, respectively. Therefore, Irgacure 819 was expected to have higher chance of succeeding in combination with 2PP. Quick *et al.* already managed to fabricate structures in the 2PP process at the micron scale with Irgacure 918 as photoinitiator.[45]

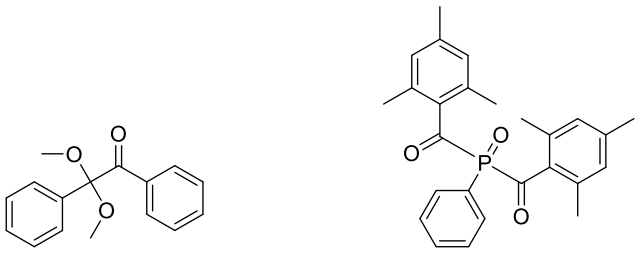

Figure 17 Chemical structures of DMPA (left) and Irgacure 819 (right)

UV-laser experiments prior to 2PP experiments are summarized in Table 2. Despite the higher concentration in DMPA (5 mol% versus 2 mol%), hardening of the droplets was reached at same time points, suggesting higher efficiency of Irgacure 819 over DMPA.

Table 2 Comparison between TRIM resins with DMPA and Irgacure 819 as photoinitiator.

Crosslinker (0.4 mL)	Photoinitiator	Concentration Photoinitiator		Time point of hardening (sec)
		mol%	wt. %	
TRIM	DMPA	5	3.5	10
TRIM	Irgacure 819	2	2.4	10

Subsequently, both resins were tested in the Nanoscribe 2PP setup. Array tests were performed to optimize scan speed (SS, µm/s) and laser power (P, % of the maximum laser power). Figure 17 shows a live image (magnification 63x) of the structures produced in the array tests for both resins. For the DMPA resin, lines, although with poor resolution, could be recognized with a 45% of the maximum laser power. Lines in the Irgacure resin could already be seen with 35% of the maximum laser power. Aiming for low laser powers to prevent material damage, it can be concluded that the Irgacure resin is more effective in crosslinking using 2PP. It should be noted that the higher contrast of the DMPA array is due to overexposure and material damage.

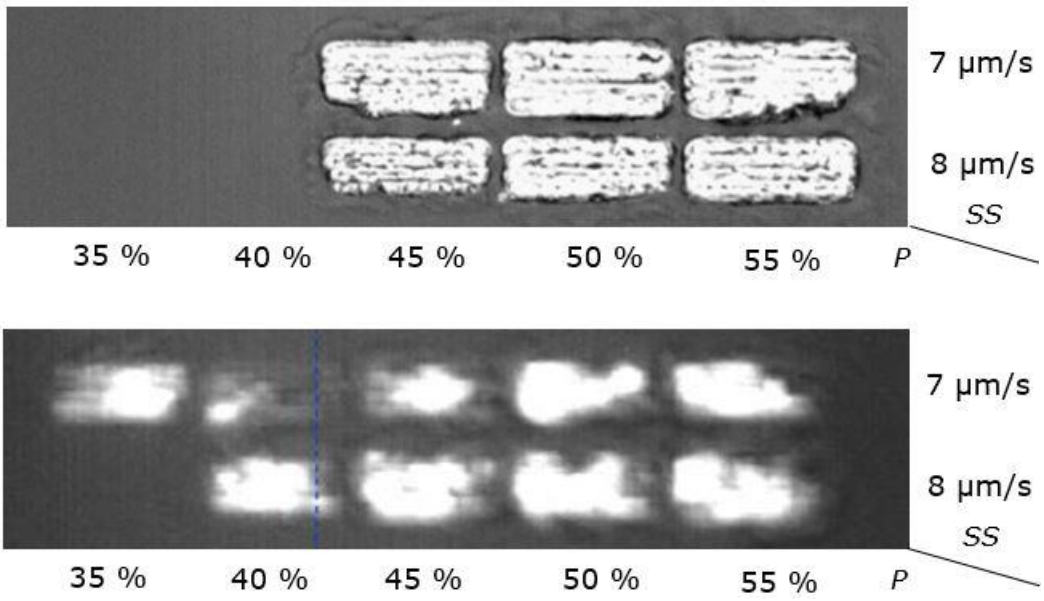

Figure 18 Live imaging on printing for parameter array test of the resin containing 5 mol% DMPA (top) and 2 mol% Irgacure 819 (bottom). For the DMPA resin, crosslinking is observed at 45% laser power (P), whereas the Irgacure 819 shows structures already at 35% laser power (P). (Magnification 63x)

Although the crosslinking of the Irgacure 819 resin was more efficient in comparison with resins containing DMPA, the resolution was still not acceptable with 2 mol% photoinitiator. Increasing the concentration of photoinitiator should improve the polymerization rate and thus the overall resolution, as was reported by Nguyen *et al.*.[18] As seen in Figure 18, a resin containing 5 mol% (5.4 wt.%) Irgacure 819 was tested in the same array test as the previous resins. In contrast to the 2 mol% (2.2 wt.%) Irgacure 819 resin, distinct lines were now observed. This result can be explained by the increased radical formation. Statistically viewed, more initiator molecules are present in the focal point of the laser and thus more molecules are prone to radical generation. Eventually, more radicals lead to a faster and more efficient crosslinking.

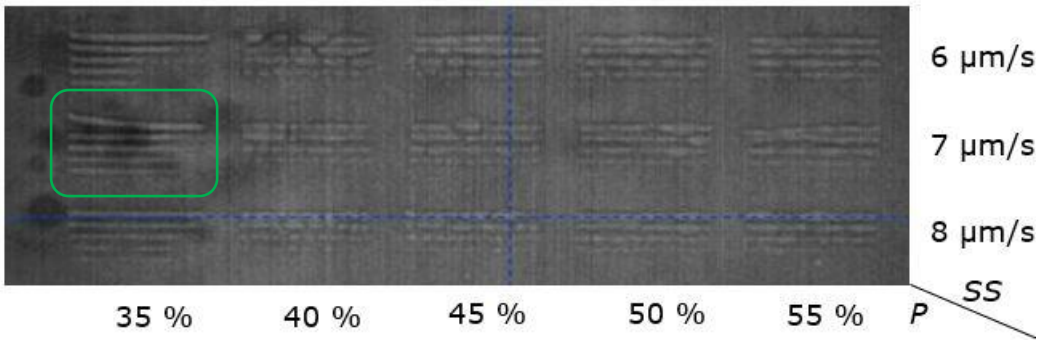

Figure 19 Live imaging on printing for parameter array test of resin containing 5 mol% Irgacure 819 in 0.4 mL TRIM crosslinker. The green square indicate the unit with the highest resolution and so the optimal laser parameter, i.e. scan speed (SS)= 7 µm/s and 35% laser power (P). (Magnification 63x)

Theoretically, higher laser powers should generate more radicals, leading to more efficient crosslinking. However, lines with laser powers higher than 35% seems to be fragmentated. This phenomena cannot be directly explained. It can be that this was just due to a locally lower photoinitiator concentration and thereby lower radical generation. Experiments should be repeated to get proper insight in this phenomena.

According to the array test, the optimal scan speed was 7 µm/s and the optimal laser power 35%. Array tests with these parameters were analyzed with the profilometer (Figure 19). Lines with a constant increase of 500 nm per line, were clearly observed. These dimensions were in agreement with the feature design.

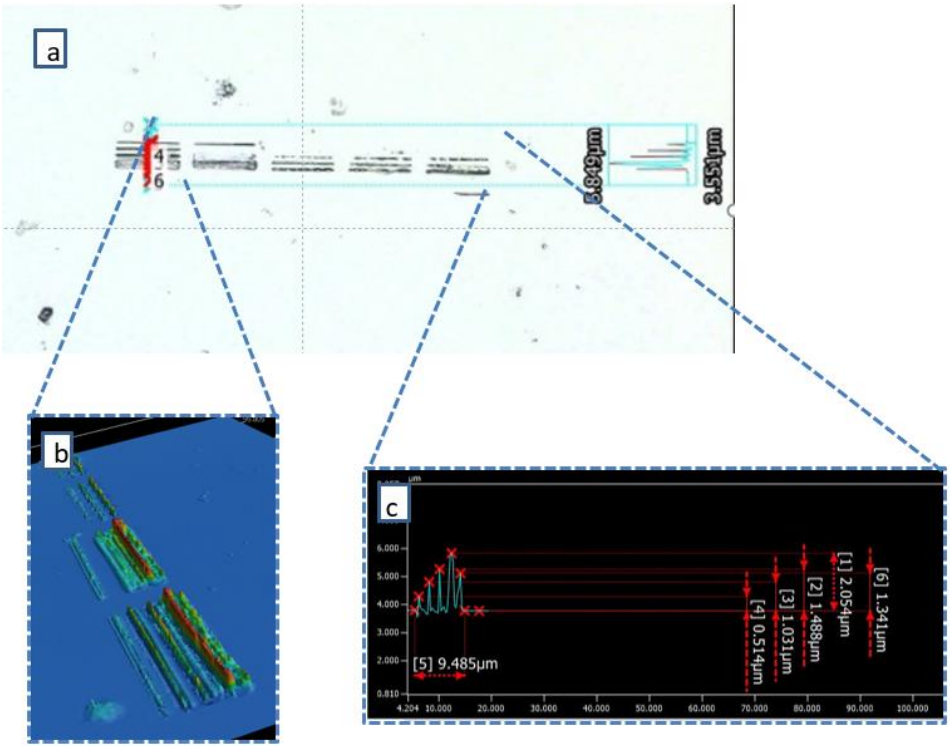

Figure 20 Profilometer analysis of the parameter array test in resin containing 5 mol% Irgacure 819 in 0.4 mL TRIM crosslinker. Scan speed 7 µm/s, Laser Power 35%. a) brightfield image of array. b) 3D profile map of the array. C) Profile of the array. Clear lines can be distinguished with a constant increasing height of 0.5 µm.

Iniferter polymers Lastly, the presence of iniferter polymers in the 2PP resins was studied. 5 mol% (5 wt. %) Irgacure 819 and 10 mol% (34 wt. %) CDP polymer (M_n = 1600 g·mol^{-1}) was dissolved in 0.2 mL TRIM (61 wt. %). To improve the solubility, 0.15 mL DMSO (43 v/v %) was added as solvent. Addition of solvent is expected to lead to a more porous structure since the molecules can act as a porogen.[46] This can affect cell behavior and could therefore be studied as an extra parameter in cell experiments. However, solvent is needed in our resins to increase polymer content and end-group concentration onto the surface of the structures.

After screening of parameter arrays, crosses of 20x20x3 micrometer could be successfully photocrosslinked with optimized laser settings (P 44%, SS 14 µm/s) at similar resolution as the commercial IP-L, i.e. a line of single voxels with spacings of 5 µm. Since polymers were added to the mixture, it was observed that higher laser powers were needed to obtain crosslinking. SEM images were taken for quality control and X-ray dispersive spectroscopy element analysis of these structures was performed for detection of carbon, oxygen, phosphor and sulfur (Figure 20). Carbon atoms can clearly be observed representing the printed shape and are mainly from the carbon skeleton of the

crosslinking monomer TRIM. The presence of oxygen in the background can be assigned to the composition of the glass substrate, whereas the small amount in the crosses is probably from both TRIM as well as the photoinitiator Irgacure 819. The possible presence of polymer could also contribute to the observed oxygen signal. A phosphor atom in the Irgacure 819 molecule explains the higher signal in the crosses over the background. Lastly, a sulfur map was obtained. A slightly higher concentration of these atoms can be seen in the cross area. This signal can be assigned to either the CDP-pMMA or to DMSO that was added for increasing the solubility. However, a resin with 2 mol% (12 wt. %) polymer instead of 10mol% (34 wt. %) showed no increased signal in the sulfur map (Figure S1), suggesting that the sulfur signal was probably derived from the presence of the increased CDP-pMMA amount.

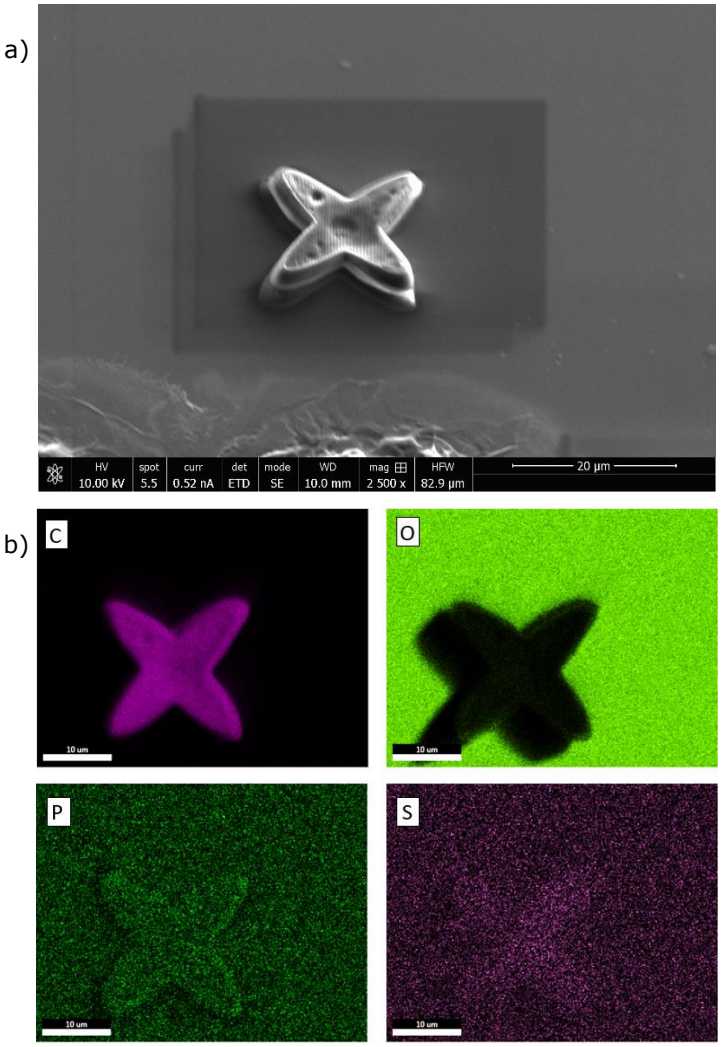

Figure 21 SEM/EDX analysis of 3D cross array. Resin composition: 10 mol% CDP polymer (1600 g·mol^{-1}), 5 mol% Irgacure 819 dissolved in 0.4 mL TRIM crosslinker and 0.3 mL DMSO *a)* SEM image of a 20x20x3 µm cross produced by 2PP. *b)* Element analysis (Carbon (C), Oxygen (O), Phosphor (P), Sulfur (S)) of 20x20x3 µm crosses *via* EDX measurements.

3.3 Polymer Post-modification

SEM/EDX analysis confirms the presence of polymers into the printed microstructures. The RAFT end-groups of these polymers make it possible to post-modify the structures. It is believed that such reactions can influence cell behavior and thereby obtain chemical control in tissue engineering applications.

A droplet of the previously described resin (10 mol% CDP polymer (1600 $g \cdot mol^{-1}$), 5 mol% Irgacure 819, 0.4 mL TRIM crosslinker and 0.3 mL DMSO) was crosslinked with conventional UV laser polymerization. A PEG-acrylate was aimed to be attached onto the polymers *via* a thiol-ene click reaction.[47] ATR-IR spectra of unmodified material, modified material and pure PEG- acrylate were measured and are shown in Figure 22. The characteristic peak of the PEG-acrylate is at 1100 cm^{-1}, which is dedicated to the C-O-C stretching vibration. In the unmodified material, this peak was not observed. However, for the spectra of the modified material, a shoulder of the 1142 cm^{-1} was seen at exactly the same wavenumber as the C-O-C peak. This finding provide strong evidence of a successful post-modification reaction.

It has to be said that, despite two washing steps with THF and isopropanol, complete removal of the unreacted PEG-acrylate cannot be guaranteed. These result should therefore be taken with caution. Further studies should focus onto extensive washing steps to ensure proper interpretation of the ATR-IR spectra.

These highlight the potential of post-modify the structures. Other chemicals can be attached onto the surface the investigate cell response and try to control cell behavior. Also, in the future, experiments in the creation of block copolymers should be done.

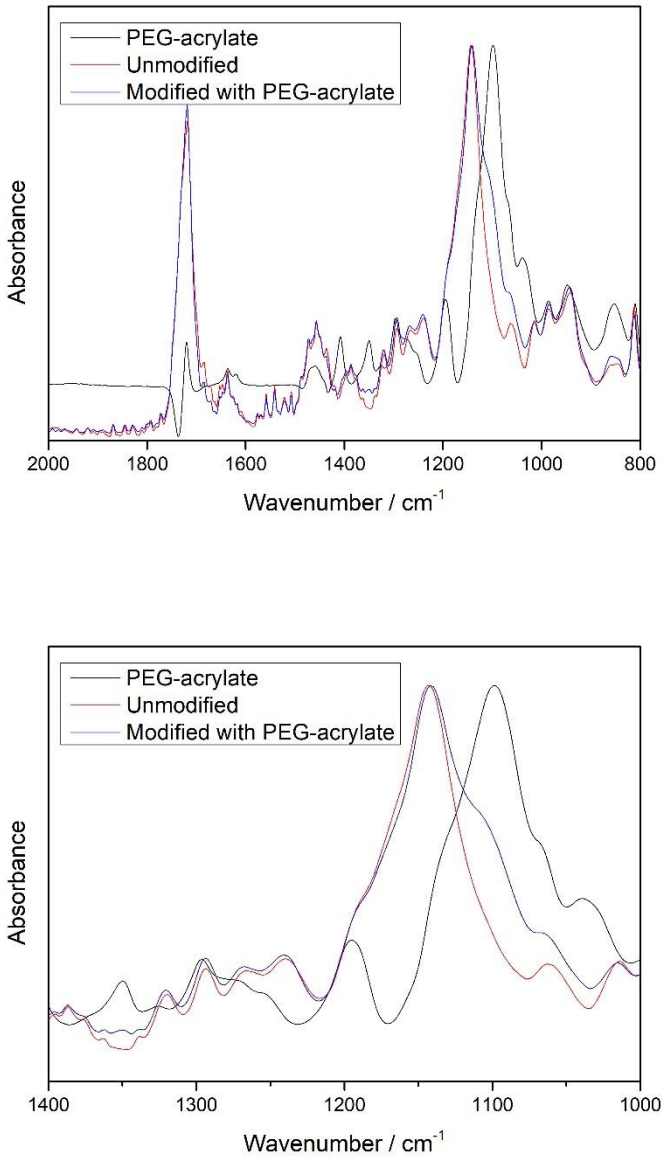

Figure 22 ATR-IR spectra of PEG-acrylate and crosslinked resin, one unmodified and one modified with PEG-acrylate. The zoomed picture visualizes the stretching vibration of the characteristic C-O-C (1100 cm^{-1}) of the PEG-acrylate.

3.4 Cell Experiments

For implementing the crosslinked resins in tissue regeneration applications, it is important to validate that the material is biocompatible. First experiments were done with crosses made from a resin without polymer content. This was done to have an indication of possible toxic effects of the mixture, especially from crosslinker (TRIM) and the 2PA photoinitiator (Irgacure 819) towards living cells. Preliminary cell studies were performed to invest cell attachment and cell viability onto the printed microstructures. This was done by seeding cells onto substrates with printed cross arrays, staining and subsequently visualizing under fluorescent microscopy.

Figure 23 shows brightfield images of the cells seeded on the microstructure array. These confirmed the presence of cells adherent onto the substrate and their ability to survive. A zoomed image from the sample shows cells in between the crosses.

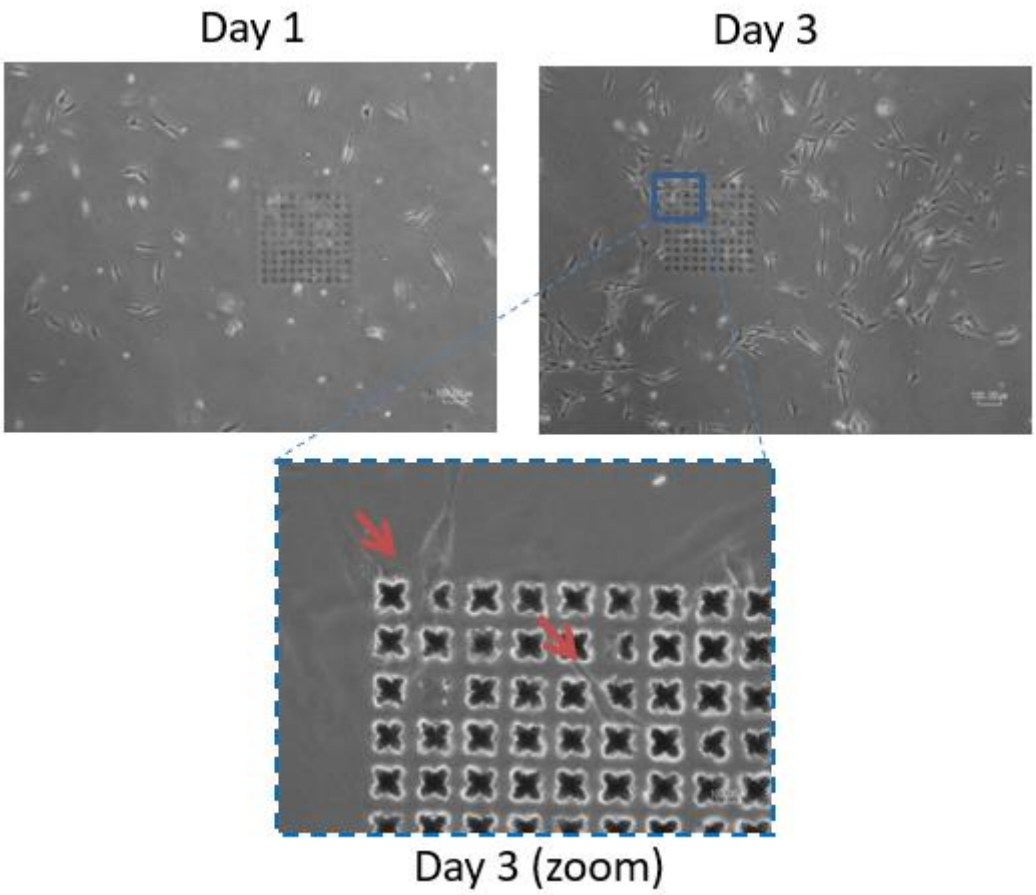

Figure 23 Brightfield image of a cross array seeded with cells after 1 and 3 day(s). The red arrows at the 'day 3 (zoom)' image indicates cell presence in the cross array. (magnification x10 (top images), 20x (Day3 (zoom)).

To asses viability of these cells, a cell viability assay was performed as live staining. Calcein AM (green) and EtD-1 (red) was used to stain livings cells and dead cells, respectively (Figure 23). Control images from areas on the substrate without a crosses indicate that the majority of the cells are alive, on day 1 as well as on day 3. For the image with the arrays after day 1, no cells can be observed in the proximity of the crosses. This can be a result of the small amount of seeded cells in the substrates. Therefore, other substrates were left in cell culture in the incubator for 9 days. At day 3, cells were presents around the crosses, as seen in the brightfield image. Fluorescence images of the same area show a high signal from the structures itself, indicating autofluorescence of the crosslinker and/or photoinitiator. However, no clear signal from the cells could be obtained. Experiment should be repeated with a higher concentration seeded cells.

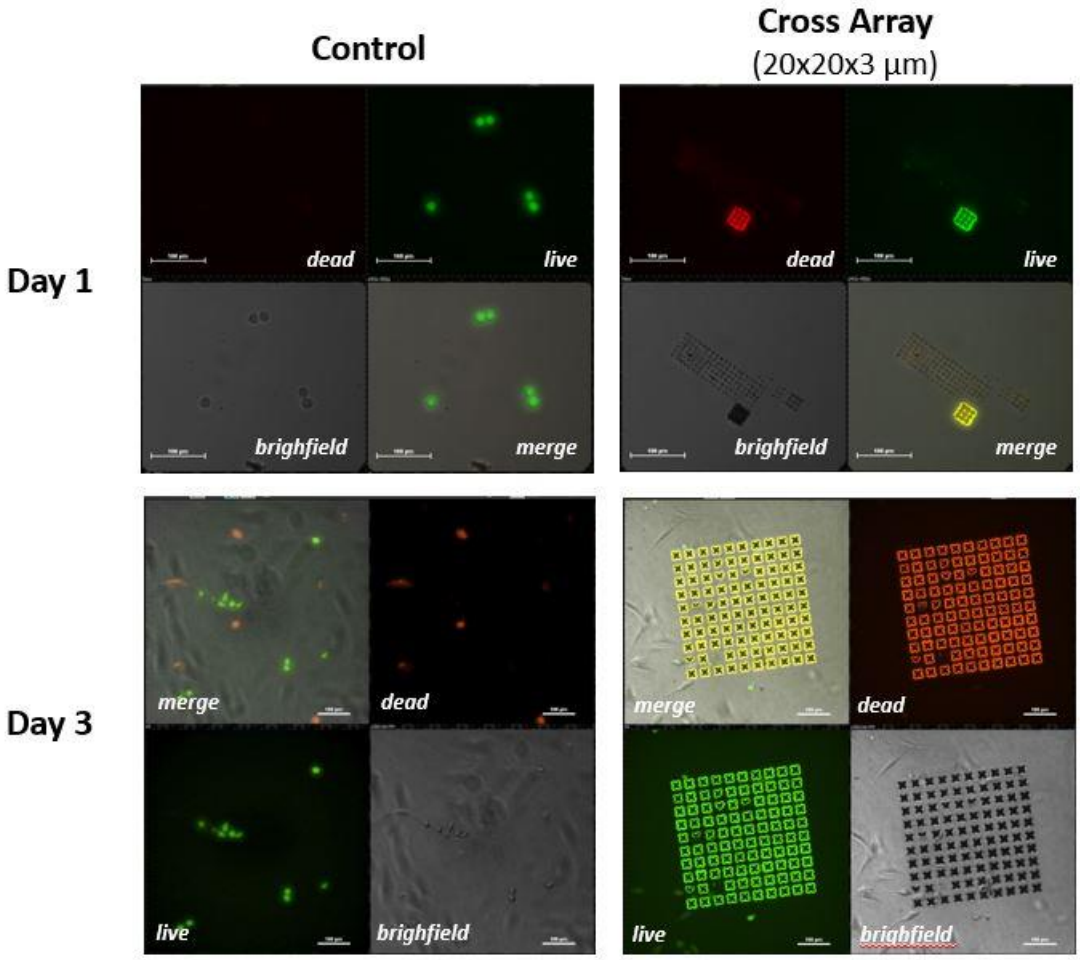

Figure 24 Fluorescent microscopy image from cell seeded cross arrays (20x20x3 crosses). Substrates are stained with Calcein AM (green) and EtD-1 (red) to visualize live and dead cells, respectively.

To better asses the attachment of the cells, staining with DAPI (blue) and phalloidin (red) was performed to visualize nuclei and actin fibers from the cytoskeleton, respectively (Figure 24). It was expected that the crosses influence the cell organization and the way they attach. This could, however, not be observed properly due to the fact that both the array and the flat control surface showed a very dense cell distribution. With this, individual contact between cells and material cannot be correctly evaluated, suggesting a lower density should be used during seeding. It is possible that the spacings between and/or the dimensions of the crosses were too small to exhibit a specific effect on cell behavior/adhesion. By screening with different dimensions and spacings, more insight into the topological control of cell growth can be evaluated.

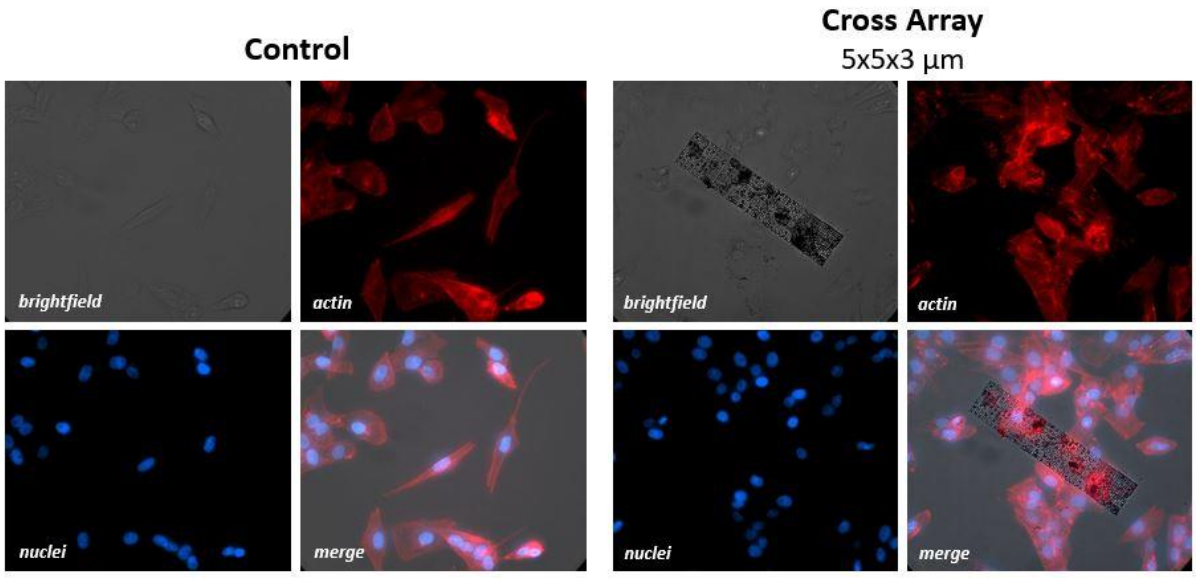

Figure 25 Fluorescent microscopy image from cell seeded cross arrays (5x5x3 crosses). Substrates are stained with phalloidin (red) and DAPI (blue) to visualize F-actin and the nuclei, respectively.

Chapter IV – Conclusion

For tissue engineering applications, it is already proven separately that both micropatterning and growth factor incorporation can have a beneficial effect in controlling cell behavior at a very small scale. In this thesis, these two principles are taken together to control cell growth. A composition of a 2PP resin which has the ability for post-modification was investigated. Besides a crosslinking monomer and an efficient 2PP photoinitiator, MMA polymers synthesized *via* an iniferter mechanism were added to the mixtures. Preferably, these polymers should be synthesized in reaction conditions that mimic the 2PP setup, i.e. UV-light and an oxygen rich environment. This to give a first indication of the behavior of the polymer in 2PP. Thanks to the controlled character of the polymerization, end-groups of the RAFT-agent should remain intact. After crosslinking of the resin in the 2PP process, the polymer end-groups cover the surface of the microstructures and are therefore accessible for all kinds of post-modification reactions, like block-copolymerization *via* the the iniferter mechanism of the polymers, thiol-ene Michael addition or esterification *via* a DCC coupling.

Photoflow iniferter polymerizations with two different RAFT-agents were investigated: a xanthate RAFT-agent and CDP RAFT-agent. The CDP RAFT-agent seemed the most suitable for this specific application. Unlike the tested xanthate RAFT-agent, polymerization of the CDP RAFT-agent with MMA in blue light displayed a linear M_n-conversion plot and relatively low Đ values, indicating a controlled behavior. On top of this, ESI-MS measurements indicate high end-group fidelity. These two features are both important for later post-modification reactions. Despite polymerizations in reaction conditions similar to the 2PP setup showed loss of control and lower end-group fidelity, it is believed that the majority of the polymers can be incorporated into the microstructures during 2PP.

A resin containing 5 mol% Irgacure 819 and 10 mol% CDP-pMMA was crosslinked during 2PP. The optimal laser power and scanning speed were 44% and 14 µm/s, respectively. Crosses of 20x20x3 µm could be produced and were characterized. Profilometer measurements confirmed the preprogrammed dimensions of the crosses. The 3D shape was also proofed by SEM images. Lastly, EDX analysis showed an increased concentration of sulfur atoms in the cross area, indicating the presence of the polymers.

First experiments in post-modification of the crosslinked resin were also performed. An aminolysis followed by an thiol-ene click with a PEG-acrylate was tested. ATR-IR showed the characteristic peak of the ether bond of the PEG-acrylate in the modified material. Further studies regarding washing steps needs to be done to properly analyze the spectra.

To give first indication of the biocompatibility of the resin, crosslinked microstructures were seeded with cells, stained and visualized in order to investigate cell attachment and viability. These results showed no significant differences in comparison with flat surfaces. In order to gain more knowledge in possible toxic effect towards cells or even topographical control of cell growth, screenings with different dimensions and/or spacings need to be done.

In summary, a 2PP resin containing iniferter polymers was developed. EDX confirms the presence of the polymers. Preliminary post-modification reactions confirms the success of the click reaction. Therefore, different systems should be explored to optimize post-modification reaction. For instance, other RAFT-agent – monomer combinations or more efficient photoinitiators could improve the final outcome. When surfaces could be successfully modified, further cell experiments should be performed. It is believed that such microstructures could lead to high control in cell behavior. In the end, this could lead to more efficient tissue regeneration. On top of this, by mimicking the *in vivo* environment, cell studies concerning physiological and pathological process could be performed more effectively.

References

[1] K. Breckwoldt, F. Weinberger, T. Eschenhagen, *Biochimica et biophysica acta* **2016**, *1863*, 1749-1759.
[2] A. Atala, (Ed.: T. TALKS), **2010**.
[3] T. Garg, O. Singh, S. Arora, R. Murthy, *Critical reviews in therapeutic drug carrier systems* **2012**, *29*, 1-63.
[4] E. Martinez, E. Engel, J. A. Planell, J. Samitier, *Annals of anatomy = Anatomischer Anzeiger : official organ of the Anatomische Gesellschaft* **2009**, *191*, 126-135.
[5] K. Duval, H. Grover, L.-H. Han, Y. Mou, A. F. Pegoraro, J. Fredberg, Z. Chen, *Physiology* **2017**, *32*, 266-277.
[6] T. Ma, Y. Li, S. T. Yang, D. A. Kniss, *Biotechnology and bioengineering* **2000**, *70*, 606-618.
[7] Z. Yang, Y. Yuan, R. Jiang, N. Fu, X. Lu, C. Tian, W. Hu, Q. Fan, W. Huang, *Polymer Chemistry* **2014**, *5*, 1372-1380.
[8] Y. S. Nam, J. J. Yoon, T. G. Park, *Journal of biomedical materials research* **2000**, *53*, 1-7.
[9] Y. S. Nam, T. G. Park, *Journal of biomedical materials research* **1999**, *47*, 8-17.
[10] S. H. Oh, S. G. Kang, J. H. Lee, *Journal of materials science. Materials in medicine* **2006**, *17*, 131-137.
[11] Q. L. Loh, C. Choong, *Tissue Engineering. Part B, Reviews* **2013**, *19*, 485-502.
[12] aF. P. Melchels, J. Feijen, D. W. Grijpma, *Biomaterials* **2010**, *31*, 6121-6130; bS. A. Skoog, P. L. Goering, R. J. Narayan, *Journal of materials science. Materials in medicine* **2014**, *25*, 845-856.
[13] aP. Tayalia, C. Mendonca, T. Baldacchini, D. J. Mooney, E. Mazur, *3D Cell-Migration Studies using Two-Photon Engineered Polymer Scaffolds, Vol. 20*, **2008**; bS. D. Gittard, R. J. Narayan, *Expert review of medical devices* **2010**, *7*, 343-356.
[14] A. Ovsianikov, B. N. Chichkov, *Methods in molecular biology (Clifton, N.J.)* **2012**, *868*, 311-325.
[15] J. Fischer, G. von Freymann, M. Wegener, *The Materials Challenge in Diffraction-Unlimited Direct-Laser-Writing Optical Lithography, Vol. 22*, **2010**.
[16] M. Malinauskas, M. Farsari, A. Piskarskas, S. Juodkazis, *Physics Reports* **2013**, *533*, 1-31.
[17] A. Ovsianikov, J. Viertl, B. Chichkov, M. Oubaha, B. MacCraith, I. Sakellari, A. Giakoumaki, D. Gray, M. Vamvakaki, M. Farsari, C. Fotakis, *ACS Nano* **2008**, *2*, 2257-2262.
[18] L. H. Nguyen, M. Straub, M. Gu, *Acrylate-Based Photopolymer for Two-Photon Microfabrication and Photonic Applications, Vol. 15*, **2005**.
[19] M. Tromayer, P. Gruber, M. Markovic, A. Rosspeintner, E. Vauthey, H. Redl, A. Ovsianikov, R. Liska, *Polymer Chemistry* **2017**, *8*, 451-460.
[20] J. Torgersen, *Efficient photoinitiators for two-photon polymerization, Vol. 2015*, **2015**.
[21] aD. M. Brunette, *Experimental cell research* **1986**, *167*, 203-217; bJ. Tan, W. M. Saltzman, *Biomaterials* **2002**, *23*, 3215-3225; cS. E. Thomson, C. Charalambous, C. A. Smith, P. M. Tsimbouri, T. Dejardin, P. J. Kingham, A. M. Hart, M. O. Riehle, *Acta biomaterialia* **2017**, *60*, 220-231.
[22] D. Barata, P. Dias, P. Wieringa, C. van Blitterswijk, P. Habibovic, *Biofabrication* **2017**, *9*, 035004.
[23] M. S. Hahn, J. S. Miller, J. L. West, **2006**.
[24] aB. Wenn, T. Junkers, *Macromolecules* **2016**, *49*, 6888-6895; bD. Cambié, C. Bottecchia, N. J. W. Straathof, V. Hessel, T. Noël, *Chemical reviews* **2016**, *116*, 10276-10341.
[25] C. J. Hawker, A. W. Bosman, E. Harth, *Chemical reviews* **2001**, *101*, 3661-3688.
[26] J.-S. Wang, K. Matyjaszewski, *Macromolecules* **1995**, *28*, 7572-7573.
[27] J. Chiefari, Y. K. Chong, F. Ercole, J. Krstina, J. Jeffery, T. P. T. Le, R. T. A. Mayadunne, G. F. Meijs, C. L. Moad, G. Moad, E. Rizzardo, S. H. Thang, *Macromolecules* **1998**, *31*, 5559-5562.
[28] aS. Perrier, *50th Anniversary Perspective : RAFT Polymerization—A User Guide, Vol. 50*, **2017**; bJ. F. Lutz, M. Ouchi, D. R. Liu, M. Sawamoto, *Science (New York, N.Y.)* **2013**, *341*, 1238149.
[29] R. N. Carmean, T. E. Becker, M. B. Sims, B. S. Sumerlin, *Chem* **2017**, *2*, 93-101.
[30] U. Ali, K. J. B. A. Karim, N. A. Buang, *Polymer Reviews* **2015**, *55*, 678-705.
[31] aL. Lemos, M. Nele, P. Melo, J. Carlos Pinto, *Modeling Methyl Methacrylate (MMA) Polymerization for Bone Cement Production, Vol. 243*, **2006**; bA. Shaik, *A Clinical Study on Outcome of Polymethyl Methacrylate Orbital Implant (Mules orbital implant) Following Evisceration, Vol. 27*, **2016**.

[32] aJ. Vandenbergh, G. Ramakers, L. Van Lokeren, G. Van Assche, T. Junkers, *RSC Advances* **2015**; bJ. Vandenbergh, T. Junkers, *Macromolecules* **2014**, *47*; cP. L. Maarten Rubens, Tanja Junkers, *Polymer Chemistry* **2017**.
[33] W. Smulders, M. J. Monteiro, *Macromolecules* **2004**, *37*, 4474-4483.
[34] H. Uk Kang, Y. Chang Yu, S. Jin Shin, J. Ho Youk, *One-Step Synthesis of Block Copolymers Using a Hydroxyl-Functionalized Trithiocarbonate RAFT Agent as a Dual Initiator for RAFT Polymerization and ROP, Vol. 51*, **2013**.
[35] V. A. Bhanu, K. Kishore, *Chemical reviews* **1991**, *91*, 99-117.
[36] M. Stenzel, L. Cummins, G. Evan Roberts, T. Davis, P. Vana, C. Barner-Kowollik, *Xanthate Mediated Living Polymerization of Vinyl Acetate: A Systematic Variation in MADIX/RAFT Agent Structure, Vol. 204*, **2003**.
[37] M. Y. Han, M.-S. Cho, Y.-J. Kwark, *Macromolecules* **2014**, *47*, 1929-1934.
[38] J. F. Quinn, L. Barner, C. Barner-Kowollik, E. Rizzardo, T. P. Davis, *Macromolecules* **2002**, *35*, 7620-7627.
[39] S. Muthukrishnan, E. H. Pan, M. H. Stenzel, C. Barner-Kowollik, T. P. Davis, D. Lewis, L. Barner, *Macromolecules* **2007**, *40*, 2978-2980.
[40] aJ. Xu, S. Shanmugam, N. Alan Corrigan, C. Boyer, *Catalyst-Free Visible Light-Induced RAFT Photopolymerization*, **2015**; bB. P. Fors, C. J. Hawker, *Angewandte Chemie (International ed. in English)* **2012**, *51*, 8850-8853.
[41] T. G. McKenzie, Q. Fu, E. H. H. Wong, D. E. Dunstan, G. G. Qiao, *Macromolecules* **2015**, *48*, 3864-3872.
[42] P. P. Database, **2015**.
[43] V. Mucci, C. Vallo, *Efficiency of 2,2-Dimethoxy-2-phenylacetophenone for the Photopolymerization of Methacrylate Monomers in Thick Sections, Vol. 123*, **2012**.
[44] K. J Schafer, J. Hales, M. Balu, K. Belfield, E. Van Stryland, D. J Hagan, *Two-photon absorption cross-sections of common photoinitiators, Vol. 162*, **2004**.
[45] A. S. Quick, J. Fischer, B. Richter, T. Pauloehrl, V. Trouillet, M. Wegener, C. Barner-Kowollik, *Macromolecular Rapid Communications* **2013**, *34*.
[46] J. Torgersen, X.-H. Qin, Z. Li, A. Ovsianikov, R. Liska, J. Stampfl, *Hydrogels for Two-Photon Polymerization: A Toolbox for Mimicking the Extracellular Matrix, Vol. 23*, **2013**.
[47] A. B. Lowe, *Polymer Chemistry* **2014**, *5*, 4820-4870.

Supporting Information

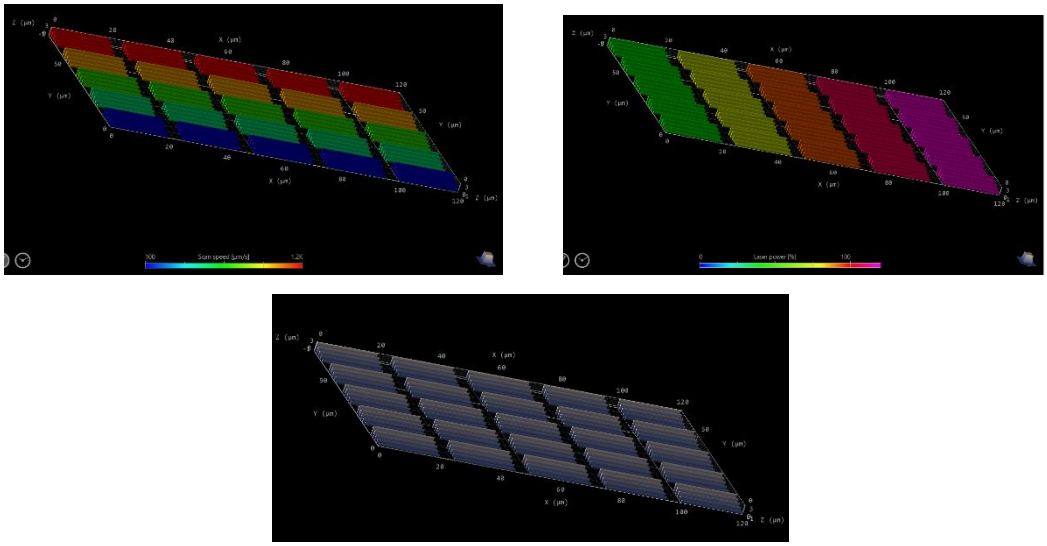

Figure S1 Preview of the printed array test in the software Describe. Laserpower was varied in the X-axis. Scanspeed was varied in the Y-axis. Each unit has 5 lines with a constant increase of 500 nm.

Table S1 Overview of resin compositions. (*DMSO was added to increase solubility)

	Crosslinker		**Photoinitiator**		**Polymer**		
Resin	*Name*	*Mol Fraction (%)*	*Name*	*Mol Fraction (%)*	*Name*	*Molecular weight ($g \cdot mol^{-1}$)*	*Mol Fraction (%)*
1	TEGDA	95	DMPA	5	/		
2	TRIM	95	DMPA	5	/		
3	TRIM	98	Irgacure 819	2	/		
4	TRIM	93	Irgacure 819	5	CDP-pMMA*	2300	2
5	TRIM	85	Irgacure 819	5	CDP-pMMA*	1600	10

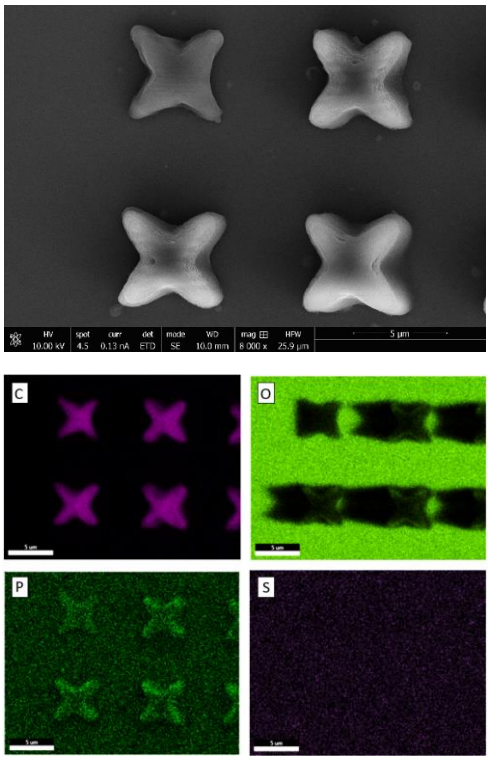

Figure S2 SEM/EDX analysis of 3D cross array. Resin composition: 2 mol% CDP polymer (2000 g·mol^{-1}), 5 mol% Irgacure 819 dissolved in 0.4 mL TRIM crosslinker and 0.3 mL DMSO *a)* SEM image of 5x5x3 µm crosses produced by 2PP. *b)* Element analysis (Carbon (C), Oxygen (O), Phosphor (P), Sulfur (S)) of 5x5x3 crosses *via* EDX measurements.

Auteursrechtelijke overeenkomst

Ik/wij verlenen het wereldwijde auteursrecht voor de ingediende eindverhandeling:
Development of Multifunctional Resins for 3D Microprinting Applications

Richting: **Master of Biomedical Sciences-Bioelectronics and Nanotechnology**
Jaar: **2018**

in alle mogelijke mediaformaten, - bestaande en in de toekomst te ontwikkelen - , aan de Universiteit Hasselt.

Niet tegenstaand deze toekenning van het auteursrecht aan de Universiteit Hasselt behoud ik als auteur het recht om de eindverhandeling, - in zijn geheel of gedeeltelijk -, vrij te reproduceren, (her)publiceren of distribueren zonder de toelating te moeten verkrijgen van de Universiteit Hasselt.

Ik bevestig dat de eindverhandeling mijn origineel werk is, en dat ik het recht heb om de rechten te verlenen die in deze overeenkomst worden beschreven. Ik verklaar tevens dat de eindverhandeling, naar mijn weten, het auteursrecht van anderen niet overtreedt.

Ik verklaar tevens dat ik voor het materiaal in de eindverhandeling dat beschermd wordt door het auteursrecht, de nodige toelatingen heb verkregen zodat ik deze ook aan de Universiteit Hasselt kan overdragen en dat dit duidelijk in de tekst en inhoud van de eindverhandeling werd genotificeerd.

Universiteit Hasselt zal mij als auteur(s) van de eindverhandeling identificeren en zal geen wijzigingen aanbrengen aan de eindverhandeling, uitgezonderd deze toegelaten door deze overeenkomst.

Voor akkoord,

Van Herck, Joren

Datum: **7/06/2018**